INL/RPT-23-75026 Rev. 000

Compare Predictions of Transient Fission Gas Release by Empirical and Mechanistic Models to Experiments in High-Burnup UO_2 Fuel

September 30, 2023

Technical Report

Pierre-Clément A. Simon[1], Larry K. Aagesen[1], Nathan Capps[2], Michael W.D. Cooper[3], Kyle A. Gamble[1], Logan H. Harbour[1], Christopher Matthews[3], Stephen Novascone[1], Daniel Schwen[1], and Brian Wirth[2,4]

[1]Idaho National Laboratory
[2]Oak Ridge National Laboratory
[3]Los Alamos National Laboratory
[4]University of Tennessee Knoxville

INL is a U.S. Department of Energy National Laboratory operated by Batelle Energy Alliance, LLC

Compare Predictions of Transient Fission Gas Release by Empirical and Mechanistic Models to Experiments in High-Burnup UO_2 Fuel

Technical Report

Pierre-Clément A. Simon[1], Larry K. Aagesen[1], Nathan Capps[2], Michael W.D. Cooper[3], Kyle A. Gamble[1], Logan H. Harbour[1], Christopher Matthews[3], Stephen Novascone[1], Daniel Schwen[1], and Brian Wirth[2,4]

[1]Idaho National Laboratory
[2]Oak Ridge National Laboratory
[3]Los Alamos National Laboratory
[4]University of Tennessee Knoxville

September 30, 2023

Idaho National Laboratory
Computational Mechanics and Materials Department
Idaho Falls, Idaho 83415

http://www.inl.gov

Prepared for the
U.S. Department of Energy
Office of Nuclear Energy
Under U.S. Department of Energy-Idaho Operations Office
Contract DE-AC07-05ID14517

Page intentionally left blank

Dedication to the late Giovanni Pastore, Ph.D.

This report is dedicated to the late Giovanni Pastore, Ph.D., former member of the BISON team. Dr. Pastore brilliantly lead the fission gases modeling efforts in BISON and spearheaded the development of the Simple Integrated Fission Gas Release and Swelling (Sifgrs) model into the leading high-fidelity capability it is today. His research and contributions established the invaluable foundations of the work presented in this report, and his impact in the field of fuel performance cannot be overstated.

Abstract

Understanding and predicting fuel performance at high burnup require improving our understanding of transient fission gas release. High-burnup operations enable new mechanisms of fission gas release, which affect fuel performance. The Nuclear Regulatory Commission has recently published its interpretation of existing fuel fragmentation, relocation, and dispersal data in a research information letter [1]. There, transient fission gas release was identified as one of the main factors that contributes to fuel fragmentation, relocation, and dispersal, and therefore limits fuel extension to high burnup. However, transient fission gas release is a complex phenomenon that cannot be fully described by simple empirical descriptions [1, 2]. This report summarizes the development of a mechanistic model for high-burnup transient fission gas release in the fuel performance code BISON. This research was supported by the Nuclear Energy Advanced Modeling and Simulation program during fiscal year 2023 to improve our understanding of high-burnup transient fission gas release and ability to predict it as a function of operation history. To support the development of a mechanistic transient fission gas release model, the existing Simple Integrated Fission Gas Release and Swelling (Sifgrs) model in BISON has been completely refactored to make it more modular and extensible. This effort supports the model's application to high-burnup conditions, its extension to other fuel forms, and the continuous improvement of its current features. Once refactoring was completed, models for high-burnup structure formation, fission gas transfer from non-restructured fuel to high-burnup structure, high-burnup structure intragranular and intergranular fission gas behavior, high-burnup structure bubble evolution, fuel pulverization, and the resulting transient fission gas release were tested and implemented in the Simple Integrated Fission Gas Release and Swelling (Sifgrs) model or tightly coupled to it. The new mechanistic model was then compared to an empirical model developed in parallel by a Nuclear Energy University Program project using a Studsvik high-burnup loss-of-coolant-accident assessment case. Finally, the report details the preliminary BISON results for a benchmark activity organized by the Nuclear Energy Agency to evaluate fuel performance codes' predictive capabilities for burst fission gas release. This work represents an important step toward a mechanistic understanding of fission gas release in high-burnup conditions.

Page intentionally left blank

Acknowledgments

This report was authored by a contractor of the U.S. Government under contract DE-AC07-05ID14517. Accordingly, the U.S. Government retains a non-exclusive, royalty-free license to publish or reproduce the published form of this report, or allow others to do so, for U.S. Government purposes. Funding was provided by the Nuclear Energy Advanced Modeling and Simulation (NEAMS) program.

This research made use of the resources of the High Performance Computing Center at Idaho National Laboratory, which is supported by the DOE Office of Nuclear Energy and the Nuclear Science User Facilities under contract no. DE-AC07-05ID14517.

Page intentionally left blank

Contents

List of Figures

List of Tables

Acronyms

AFC	Advanced Fuels Campaign
CEA	French Alternative Energies and Atomic Energy Commission
Cr	cromium
FFRD	fuel fragmentation, relocation, and dispersal
FGR	fission gas release
HBS	high-burnup structure
HBu	high burnup
Sifgrs	Simple Integrated Fission Gas Release and Swelling
LOCA	loss-of-coolant accident
LWR	light-water reactor
MD	molecular dynamics
MOOSE	Multiphysics Object-Oriented Simulation Environment
NEA	Nuclear Energy Agency
NEAMS	Nuclear Energy Advanced Modeling and Simulation
NEUP	Nuclear Energy University Program
NR	non-restructured
NRC	Nuclear Regulatory Commission
PIE	post-irradiation examination
tFGR	transient fission gas release
U_3Si_2	uranium silicide
UCO	uranium oxycarbide
UN	uranium nitride
UO_2	uranium dioxide
Xe	xenon

1. INTRODUCTION

1.1 Context of the Milestone

As the U.S. nuclear energy industry continues to investigate and identify strategies to further reduce the energy production costs for the existing fleet of nuclear-power–generating stations, utilizing fuel at higher burnup to reduce fuel costs is of great interest. However, fuel fragmentation, relocation, and dispersal (FFRD) remain a concern. The Nuclear Regulatory Commission (NRC) has recently published its interpretation of existing FFRD data in a research information letter [1]. There, tFGR was identified as one of the main factors contributing to FFRD and therefore limits the extension to HBu. Among other things, fission gases lead to significant fuel microstructural changes, affect the thermal conductivity of the fuel and rod gap and plenum, and contribute to fuel swelling, cracking, fragmentation, and pulverization under normal and transient operations. It therefore also contributes to fuel relocation, dispersal, and LOCA conditions [1, 3]. Understanding and predicting fuel performance thus require understanding and predicting fission gas behavior.

However, tFGR is a complex phenomena that cannot be fully described by simple empirical descriptions [1, 2]. The sparse experimental data does not show clear and quantifiable trends, and current empirical approaches are either extremely conservative or can only be applied to very specific cases limiting the use of empirical approaches for predictive fuel performance modeling and safety analysis. The industry lacks a predictive, mechanistic model able to cover a wide range of operation and LOCA conditions. However, accurately predicting tFGR requires not only an adequate description of all its mechanisms but also a precise prediction of all the mechanisms that lead up to tFGR, namely fission gas generation, intragranular and intergranular behavior, bubble evolution, and other mechanisms of FGR. This report details Nuclear Energy Advanced Modeling and Simulation (NEAMS) efforts to develop such a model.

1.2 Introduction to Sifgrs

Sifgrs is a state of the art fission gas behavior and swelling model implemented in BISON and is used to support this milestone. It was first focused on UO_2 for low-burnup fuel during normal operations and was expanded to transient conditions and other fuel forms such as chromium-doped UO_2 and U_3Si_2 through the NEAMS program. Under the late Giovanni Pastore's stewardship, it became a reference for fission gas modeling and one of the strengths of the fuel performance code BISON.

Sifgrs employs a generally mechanistic approach to simulate fission gas behavior and describes different steps of

fission gas transport and eventual release. At the start of this fiscal year (FY), it already proposed leading capabilities for intragranular fission gas modeling [4, 5, 6, 7, 8, 9, 10, 11, 12], described intergranular fission gas behavior in the form of lenticular bubbles with coalescence criteria [4, 10], and accounted for diffusional release and burst release due to microcracking of fuel during temperature transients [13]. To describe all the different aspects of its model, Sifgrs leveraged a mix of empirical, semi-empirical, and mechanistic models—some of them based on atomistic simulations [14, 15]. This flexible approach lends itself to accelerated model development and continuous model improvement as more insight is gained on different aspects of the model. Sifgrs, as a part of BISON, contributes to improving our understanding of fuel performance modeling.

Sifgrs, however, did not offer significant HBu capabilities to address the needs described above. NEAMS aims to develop a mechanistic tFGR model and provide valuable insight on fission gas behavior in HBu conditions. To that end, we aim to add existing HBu models to Sifgrs and combine with new model developments to propose a new mechanistic tFGR model.

Unfortunately, since its start more than 10 years ago, Sifgrs grew organically and acquired a plethora of interconnected models with an array of parameter options, which made its implementation particularly complex and prohibitively challenging to modify. This complexity has stalled its development in the past few years. Indeed, recent fission gas model developments have been done outside of Sifgrs to escape its complexity. Unfortunately, this leads to inconsistencies (such as fission gas mass loss or gain) since these models should all be coupled under Sifgrs. This situation prevented Sifgrs from being extended beyond its current capabilities to address the current needs of the nuclear industry. Today, the needs to expand the applicability of Sifgrs to more fuel forms and add extensive HBu capabilities require a refactoring of the code.

1.3 Aims of the Milestone

The overarching goal of the milestone is to develop a new tFGR model. Following the language of the milestone, this model should be based on bubble populations and bubble pressures in the fuel, which is sensitive to the fuel microstructure and operating conditions. To prevent inconsistencies, the model should support an integrated approach that combines the existing Sifgrs model for lower burnup fuel with a newly developed model for HBS fuel from the literature [16]. The new model should also leverage the existing pulverization criterion for HBu fuel [17, 18, 19].

To integrate these models, the existing Sifgrs code was planned to be refactored to increase modularity and extensibility. This refactoring effort was scheduled to support other NEAMS milestones and Nuclear Energy University Program (NEUP) projects, namely the implementation a version of Sifgrs for uranium nitride (UN) fuel, and the development of an empirical tFGR model. The implementation of the mechanistic model of transient fission gas release can focus on the HBS located in the rim of the fuel but should be extendable to other parts of the fuel to prepare future work on the dark zone [20].

The last aim of the milestone was that the mechanistic models should be benchmarked against models of more empirical nature. The results of these models should be evaluated against existing HBu experimental data. This milestone should therefore also assess the impact of tFGR modeling on existing validation cases where tFGR was not measured.

1.4 Organization of the Milestone

The current report describes how each of these goals have been met. The different sections address different aims listed above. Therefore, the organization of this report is as follows. In Chapter 2, we detail Sifgrs's refactoring. We describe the main motivations behind this important endeavor and establish the main implementation goals. Then, we detail all the major changes in Sifgrs's implementation, as well as the main bugs that were fixed and improvements that were made in the process. In Chapter 3, we detail the development of the new tFGR model in Sifgrs. This chapter therefore includes a description of HBS formation, fission gas transition from NR fuel to HBS fuel, intragranular and intergranular HBS fission gas behavior, HBS bubble evolution, pulverization, and the resulting tFGR. In Chapter 4, we compare the empirical tFGR model developed in Ref. [21] and the new mechanistic model. We describe the features of both models and use a Studsvik LOCA case to quantify their differences in FGR predictions. In Chapter 5, we describe a benchmarking activity led by NEA to compare different fuel performance codes in transient conditions representative of anticipated operational occurrences. The goals of the benchmarking activity are to enhance the understanding of burst FGR mechanisms and facilitate the improvement of fuel performance code models for transient conditions (or develop new ones), reducing uncertainties and increasing margin to fuel performance limits. We describe preliminary BISON predictions and comment on its accuracy based on comparison against experimental measurements. We then conclude the report in Chapter 6.

2. REFACTORING OF THE Sifgrs IMPLEMENTATION IN BISON

2.1 Refactoring Goals

Sifgrs was first developed more than 10 years ago and grew organically since then. It was first focused on UO_2 for low-burnup fuel during normal operations and was expanded to transient conditions and other fuel forms such as chromium-doped UO_2 and U_3Si_2 through the NEAMS program. Under the late Giovanni Pastore's stewardship, it became a reference for fission gas modeling and a highlight of the fuel performance code BISON. Today, the needs to expand the applicability of Sifgrs to more fuel forms and add extensive HBu capabilities require a refactoring of the code. Having grown organically, the addition of new capabilities was making Sifgrs exponentially more complex, which has stalled its development in the past few years. As will be discussed below, new models of fission gas behavior were recently added to BISON outside of Sifgrs because of its daunting complexity. The main goals of the refactoring are listed as:

- Increase modularity to enable the accelerated development of new models for UO_2 Sifgrs, such as HBu capabilities, and to rapidly apply Sifgrs to new fuel forms: UN and uranium oxycarbide (UCO) for example
- Decrease code duplication, which simplifies and accelerates code maintenance and minimizes the divergence of capabilities that should remain identical
- Increase code readability by using common naming schemes and increasing in-code documentation
- Increase documentation of Sifgrs's capability in the BISON documentation, especially crucial for users without source access
- Increase guardrails against the concurrent use of inconsistent models
- General clean up of potential bugs or confusing aspects of Sifgrs' implementation.

These goals guided the efforts described in this section.

2.2 Refactoring Approach

Properly refactoring a code as complex as Sifgrs requires a clear, effective, and flexible plan. Sifgrs has been established as one of the most advanced fission gas capabilities—thanks to the contributions of Dr. Giovanni Pastore and collaborators—and has been widely used by industries and research institutions. It is therefore paramount that the effort to refactor Sifgrs does not affect its performance in any unexpected and/or negative ways. In other words, users should not observe unexpected changes in their simulation predictions as a result of refactoring this code. To balance this quality control constraint with the need to rapidly and profoundly refactor Sifgrs to reach the aims listed above, a thorough plan was establish before changing the code:

1. **Understanding the current code structure and interactions between different parts:** Listing the current capabilities, as well as understanding the current implementation of the code—with all its interactions—is a crucial step to evaluate the starting point of the refactoring process. The code structure was detailed and recorded. An example of this is shown in Fig. 2.2a.
2. **Design a new code structure:** Before making significant changes to Sifgrs, a clear final code structure was designed to develop an overarching vision of the end goal. This is crucial to effectively refactor the code in ways that align with the final goal. Note that although it is important to design a final structure early in the process to guide refactoring, flexibility is paramount to solve unexpected difficulties and readjust as understanding and needs evolve.
3. **Increase test coverage (calculated by GitHub):** To ensure that the refactoring effort in Sifgrs does not affect its performance in any unexpected and/or negative ways, test coverage has been greatly improved prior to making significant changes.
4. **Prioritize changes:** As a complex, intricate code, the Sifgrs implementation has many interacting pieces that depend on each other. Properly prioritizing changes helped with the effective execution of the refactoring process. Moreover, many other NEAMS milestones (development of HBS formation model, UN fission gas capabilities, etc.) and NEUP projects relied on parts of Sifgrs being ready on time for their implementation. These dependencies were accounted for to prioritize different aspects of the refactoring process.
5. **Implement changes step by step, ensuring that none of the tests or assessment cases were unexpectedly affected by these changes:** The NQA-1 compliant testing capabilities and process used in GitHub for the development of BISON were leveraged to track the effect of any changes made to Sifgrs. In particular, the new ability to run assessment cases was used to prevent unexpectedly breaking or affecting them.
6. **Changes to fix bugs or correct models:** Part of Sifgrs' refactoring consists of checking existing model implementations, which the increased test coverage facilitates. Fixes, which would positively affect test results, were done separately from any structural change to prevent undetected consequences of refactoring.

2.3 Description of Sifgrs's refactoring

2.3.1 Increased test coverage

The first step of the refactoring process was to increase test coverage of the Sifgrs implementation. The percentage of test coverage by line corresponds to the percentage of lines of code being run by tests. It is calculated in GitHub each time a new contribution is made to BISON. Having a high percentage of test coverage provides confidence that any changes in model behavior and prediction resulting from refactoring will be captured by tests, thus limiting unintended changes. New carefully designed tests were added to BISON to increase test coverage in Sifgrs. During this effort, test coverage increased from around 80.6% in February 2022 to 95.1% at the end of FY 2023. This significant improvement ensures the reliability of the Sifgrs implementation and has help identify issues, as detailed in Section 2.4.

In parallel, existing tests were modified to output more material properties calculated by Sifgrs, which enables a more extensive tracking of behavior and prediction changes resulting from modifications to the code. Moreover, new tests were updated or created to verify the implementation of some of the models used in Sifgrs. Although test coverage by line is important, test coverage by modeling capability is crucial to developing and maintaining a reliable, verified model implementation. Some of these new tests are discussed in Section 2.4.

2.3.2 Consistent naming scheme

Sifgrs involves a large amount of variables and materials properties from temperature to amount of fission gas in bubbles pinned at dislocations and numerical parameters for algorithms such as PolyPole2. This list evolves and grows as new capabilities are being added to Sifgrs and currently consists of around 200 different variables and material property names. With so many different names, it is crucial to use a consistent naming scheme across the implementation to avoid errors and confusion. Moreover, the units of each value and a short description of the entity should be easily available to users and code developers. An important part of refactoring Sifgrs consisted of renaming variables, parameters, and materials properties which had inconsistent or non-descriptive names and documenting their units and definition. For example, `atm_per_bbl_disl`, `atoms_per_bubble_at_dislocation`, and `atm_bbl_disl_grn_3`, which all represented the number of atoms per intragranular bubble at dislocations, were renamed `atom_per_bubble_intra_dislocation`. This effort made the Sifgrs implementation easier to understand and follow, therefore reducing the barrier to entry and the likelihood of bugs. In particular, these changes helped identify some of the typos and bugs discussed in Section 2.4. The list of previous names and the corresponding new names along with the units of each property/variable and a short description is available at https://bison-discourse.hpc.inl.gov/t/important-update-in-naming-convention-of-variables-and-material-properties-in-sifgrs/137.

2.3.3 Use of PhysicalConstants

In BISON, the value of some commonly used constants such as the gas constant or the Avogadro's number have been listed in `PhysicalConstants.h` to be used anywhere in BISON. This enables the use of consistent values for these important constants across the code and not relying on locally defined values with arbitrary—and inconsistent—numbers of significant digits or approximations. The constants from `PhysicalConstants.h` replaced all of the locally

defined constants used in Sifgrs for consistency.

2.3.4 Use of consistent parameter values

Some model parameter values were defined in different places in the code with different local values. As discussed in Section 2.3.3 for physical constants, doing so leads to inconsistent model results. One example of this was the definition of the surface energy between fuel and gas, with three different values being defined at three different places in the code for UO_2: 0.5 J/m^2 by default as user input, 0.7 J/m^2 in `IntraGranularFissionGas` for calculating the radius of bubbles pinned at dislocations, and 1.0 J/m^2 in the model calculating the intragranular bubble radius. This means that even if a user provided a different value from 0.5 J/m^2, the other values would remain unchanged. Similarly for U_3Si_2, different values were used in different parts of the code. This inconsistency is especially detrimental to model predictions, as surface energy has been identified as one of the model parameters that most strongly influence swelling and fission gas release [10].

This issue was fixed with three objectives in mind: (1) the value should be defined once in each fuel-specific Sifgrs (i.e., once in `U3Si2Sifgrs` and once in `UO2Sifgrs`) and be used consistently everywhere, (2) the value could be user-defined, and (3) the default value should correspond to current estimates of this property. For UO_2, Hall et al. recommend a temperature-dependent surface energy value, $0.85 - 1.4 \times 10^{-4} T$ J/m^2, and acknowledge that measurements errors can be as large as 70% [22]. Later, Kogai published a value of 1 J/m^2 [23]. The default surface energy value was therefore defined as 0.85 J/m^2 in `UO2Sifgrs`. For U_3Si_2, values around 1.16-1.43 J/m^2 had been published in Ref. [24, 10]. These values were obtained by deriving the surface energies of a series of surfaces with various Miller's indices. An updated value of 1.7 J/m^2 was published in Ref. [25] using molecular dynamics (MD) simulations to determine the surface energy for a void in U_3Si_2 fuel. The new default value in `U3Si2Sifgrs` was therefore set to 1.7 J/m^2.

Once these changes were implemented, the affected tests and assessment cases in BISON were updated. In general for UO_2, it led to a slight increase in FGR, which is often underestimated. However, the principal contribution from this change is not a net improvement in BISON's predictive ability but an increase in the consistency of Sifgrs' implementation and flexibility for users.

2.3.5 Refactoring of `IntragranularFissionGas.h` and `Sifgrs.h/.C`

The previous implementation of Sifgrs consisted of the namespace `IntragranularFissionGas.h`, which handled all the intragranular behavior for UO_2 (doped and undoped) and U_3Si_2, and the Sifgrs class itself, which handled intergranular fission gas behavior and release for every fuel type. In addition to a large amount of code duplication, having different models for each material directly in `IntragranularFissionGas.h` and the Sifgrs class led to a large number of options for material models that were not compatible across fuel forms. This implementation made option tracking—ensuring incompatible options are not used together—exponentially complex as the number of fuel forms and models increased. For example, adding a model for intragranular bubble growth for UN, which was needed for the NEAMS project described in Ref. [26], required creating new options in each relevant function and adding numerous warnings and error messages ensuring that this UN model could not be inadvertently used to model UO_2 or U_3Si_2. As

Sifgrs's capabilities are extended to new fuel forms and informed by new models, such as HBu models, it is crucial to limit code duplication and the complexity of option tracking. To that end, both `IntragranularFissionGas.h` and `Sifgrs.h/.C` were refactored.

`Sifgrs.h/.C` was turned into a series of fuel-type-focused classes all relying on a base class that regroups the shared model implementation. The base class—`SifgrsBase`—contains all the basic model implementations that are shared by several fuel type. Material-specific models and parameters values are now implemented in material-specific class that inherit from the base class. The material-specific classes are named `UO2Sifgrs`, `U3Si2Sifgrs`, and `UNSifgrs`. Each material-specific class has their own separate options, which by design cannot inadvertently be used in other fuel forms.

The namespace `IntragranularFissionGas.h` was turned into a class, and (as was done with Sifgrs) material-

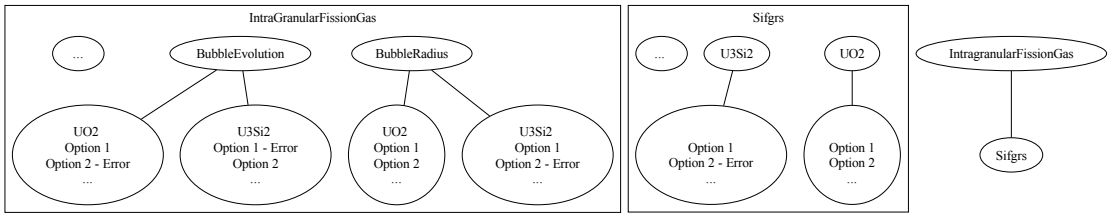

(a) Previous implementation

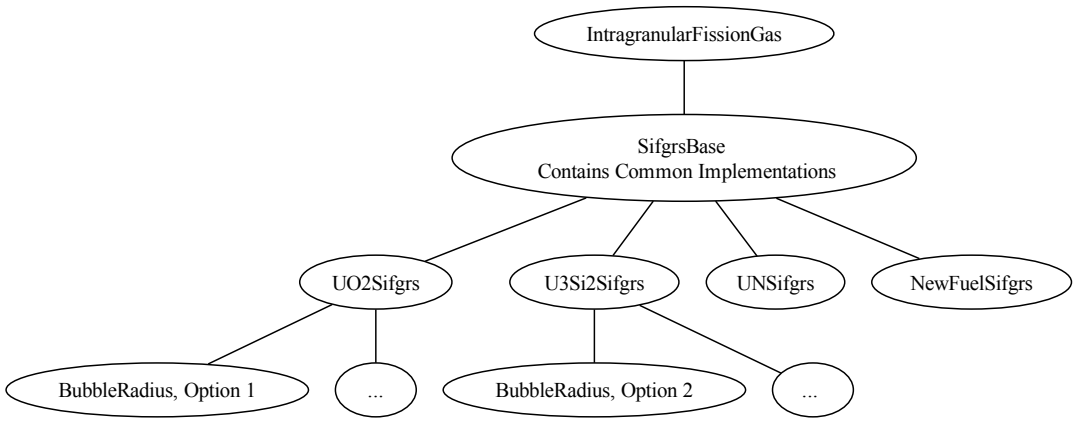

(b) Updated implementation

Figure 2.1. Diagrams contrasting the (a) previous and (b) updated Sifgrs implementation in BISON. `IntraGranularFissionGas` and `SifgrsBase` now contain the common model implementation, and dedicated material classes focus on material specific models and parameter values. This implementation reduces code duplication, naturally handles option tracking, and increases modularity.

specific models and parameter values have been moved to material specific classes. The intragranular capabilities implemented in the `IntragranularFissionGas` class are now inherited by `SifgrsBase`, which can then be used in material-specific classes (`UO2Sifgrs`, `U3Si2Sifgrs`, and `UNSifgrs`). A diagram contrasting the previous and updated Sifgrs implementation is available in Fig. 2.1.

Having separate material-specific classes inherit from `SifgrsBase` of `IntragranularFissionGas` significantly reduces code duplication and removes the need for option tracking across fuel types, therefore reducing maintenance cost and the occurrence of bugs. Moreover, it increases modularity and accelerates code development as common functions can be leveraged from the base class rather than implemented anew. The rapid implementation of `UNSifgrs` shows how much more modular and flexible the `Sifgrs` implementation became [26].

2.3.6 Refactoring of the main function in IntragranularFissionGas.h

Sifgrs' capabilities to model intragranular fission gas behavior are rich [4, 27, 8, 11, 12, 9, 13]. Moreover, it offers great flexibility in modeling choices—from selecting the bubble evolution model to choosing the coefficients of atomic diffusion. Although specific models are implemented in individual functions (e.g., `BubbleRadius` and `AtomicDiffusionCoefficient`), the overall fission gas behavior is handled by a function called `Behavior`. As Sifgrs grew in capabilities and complexity, so did the implementation of `Behavior`, with a large number of options being added over time. As a result, `Behavior` had become a very complex function difficult for anyone new to Sifgrs to fully understand. The structure of `Behavior` prior to refactoring is shown in Fig. 2.2a. This barrier to entry made it challenging to properly add new intragranular capabilities to Sifgrs and risked slowing down its development and applicability to new fuel forms.

`Behavior` was therefore refactored to focus on the physics and common steps for intragranular fission gas modeling, which streamlined the code structure and reduced code duplication. The updated structure of `Behavior` is shown in Fig. 2.2b, with three main functions used to represent the three main steps of the algorithm, namely `BehaviorBubbleEvolution` to determine the concentration of intragranular bubbles, `BehaviorNumericalAlgorithm` to leverage either Formas, PolyPole1, or PolyPole2 to solve the equations of intragranular fission gas behavior, and `BehaviorBubbleRadius` to determine the intragranular bubble radius. Since the previous implementation was focused on the options rather than the physics, a result of the organic growth of Sifgrs, these common algorithmic steps were easily lost on code developers (see Fig. 2.2a). The options themselves are now used within these three new functions, and a reader can clearly identify their impact on the physics and potentially add new capabilities. The structures of `BehaviorBubbleEvolution`, `BehaviorNumericalAlgorithm`, and `BehaviorBubbleRadius` are shown in Fig. 2.3.

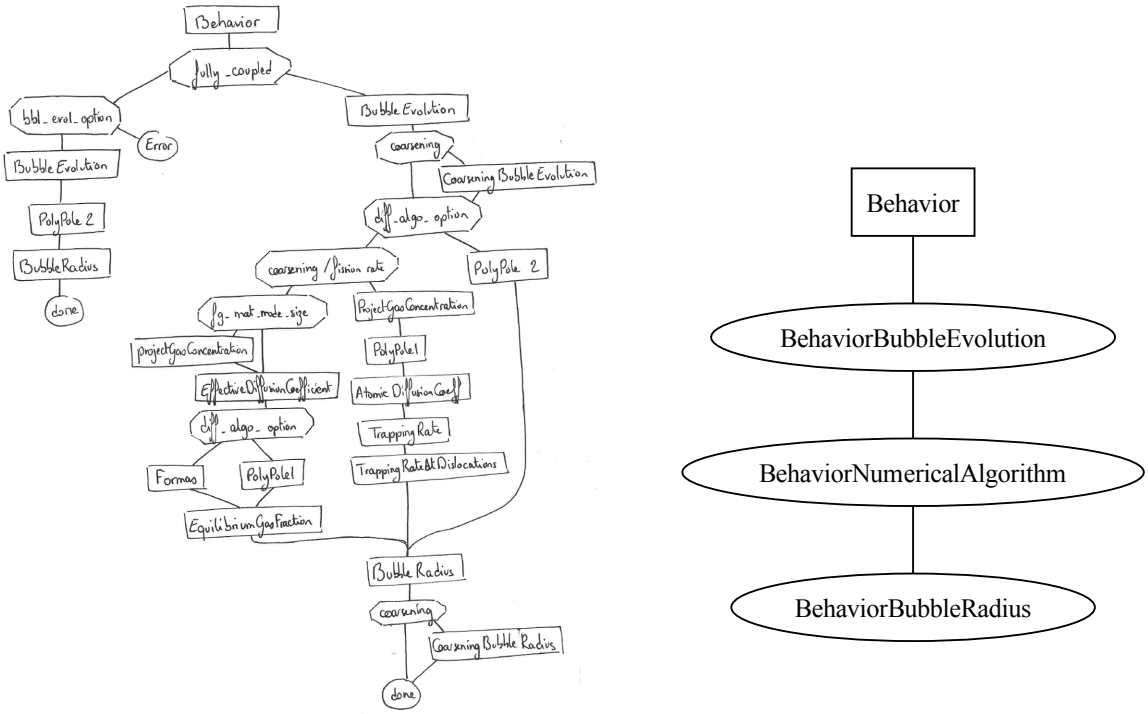

(a) Previous implementation

(b) Updated implementation

Figure 2.2. Diagrams contrasting the (a) previous and (b) updated implementation of the `Behavior` function in `IntraGranularFissionGas` in BISON. The updated implementation is focused on the physics and the common steps of intragranular fission gas modeling, which streamlines the code structure and reduces code duplication.

2.3.7 Refactoring of HBS formation capabilities

Several models are available in BISON to model HBS formation. Although a NEAMS effort is underway to develop a lower length scale model of HBS formation, the two currently available models originate from Lassmann et al. [28] and Barani et al. [16]. Both of them compute, although in different ways, the amount of restructured fuel at the rim periphery. However, the implementations of the two models were not consistent. The Lassmann model was implemented directly in Sifgrs; the Barani model was implemented in the dedicated `HighBurnupStructureFormation` class. Because the two classes did not communicate, a user could potentially be using both inconsistent models at the same time and get results corresponding to neither model. Moreover, this limited Sifgrs to use only the Lassmann model rather than the more recent and predictive Barani model.

To avoid the concurrent use of competing models and expand Sifgrs' capabilities, both models calculating the fraction of restructured HBu fuel were moved to the `HighBurnupStructureFormation` class, and calculations related to fission gas behavior are performed in `UO2Sifgrs` (no HBS fission gas capabilities are yet available in BISON for other fuel forms, so these calculations are specific to UO_2). To ensure coordination between the two classes, `UO2Sifgrs` reads which HBS formation option was defined by the user (`Lassmann` or `JMAK_Barani`) and the calculated volume

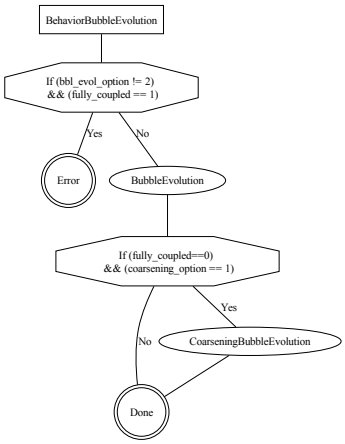

(a) `BehaviorBubbleEvolution`

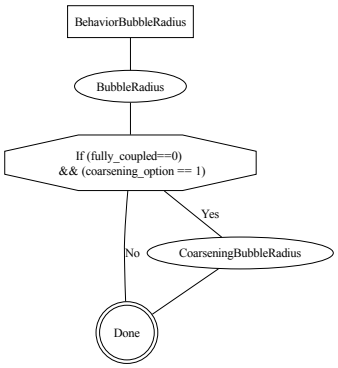

(b) `BehaviorBubbleRadius`

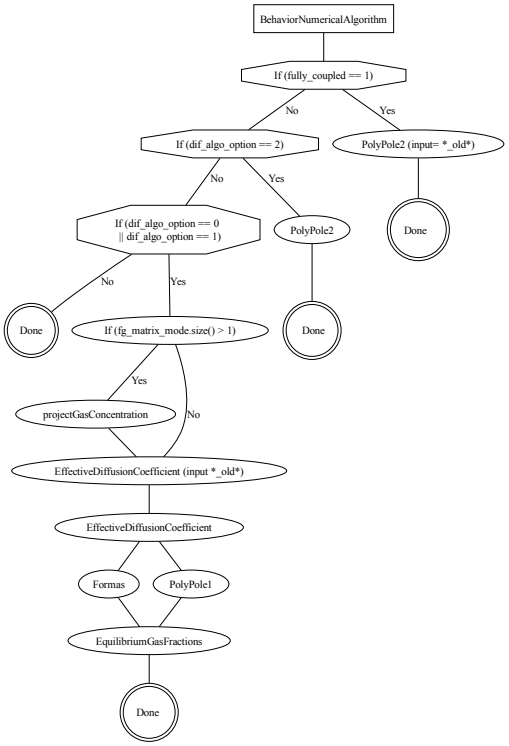

(c) `BehaviorNumericalAlgorithm`

Figure 2.3. Diagrams of (a) `BehaviorBubbleEvolution`, (b) `BehaviorBubbleRadius`, and (c) `BehaviorNumericalAlgorithm`, the three steps of the `Behavior` function in `intraGranularFissionGas`.

fraction of HBS from `HighBurnupStructureFormation`. This way, both classes communicate and HBS calculations are consistent across classes. Moreover, adding new models for HBS formation and fission gas behavior in restructured fuel is made straightforward with limited code duplication.

Predicting fuel pulverization is an important part of fuel performance modeling at HBu and has been the focus of several NEAMS milestones [18]. These efforts led to the development of the `UO2PulverizationMesoscale` class, which calculated the radius and pressure of HBS bubbles and determined the fraction of pulverized fuel. Unfortunately, this class was very loosely connected to Sifgrs, which led to code duplication and lack of consistency. Different models could be simultaneously used for HBS bubble evolution, and the amount of generated fission gas was counted twice (once in `Sifgrs` and once in `UO2PulverizationMesoscale`), resulting in an overestimation of fission gas amount. More details on how the amount of generated fission gas was counted twice (or more) are available in Section 2.4.5. After Sifgrs was refactored, it became feasible to consolidate the capabilities from `UO2PulverizationMesoscale` and `UO2Sifgrs` and ensure a consistent treatment of fission gas in low and HBu fuel. The extensive development of fission gas modeling capabilities for HBS in Sifgrs is the focus of Section 3.2.

2.3.8 Use of Enums to reduce confusion around options

Sifgrs combines a large number of options for different models. For example, options exist to select either Formas [5], PolyPole1 [11], or PolyPole2 [8] to solve the intragranular fission gas behavior equations. Until now, all these options were defined using integers. For example, `ig_diff_algorithm = 0` would call Formas, `ig_diff_algorithm = 1` would call PolyPole1, and `ig_diff_algorithm = 2` would call PolyPole2. Although a reasonable approach for a few options, using integers as options is not explicit and can lead to confusion—especially when using as many options as Sifgrs does. Moreover, the same integer options were used across different fuel forms, even though models were very different. For example, `diff_coeff_option=0` would correspond to athermal vacancy diffusion from Ref. [29] in UO_2, but to a mechanism of U vacancy self-diffusion along the c-axis from Ref. [15] in U_3Si_2.

To reduce confusion and make these options more explicit and user friendly, the `MOOSE::ENUM` are being used instead of integers. This gives options explicit names and better tracks them. Table 2.1 lists the previous and updated modeling options; Tables 2.2 and 2.3 list the previous and updated parameter options; Table 2.4 lists the previous and updated transient options. Note that the references listed in Tables 2.1 to 2.4 for each relevant option is now also documented within the Sifgrs implementation.

The changes have been documented and communicated to users on https://bison-discourse.hpc.inl.gov/t/enum-options-replace-integer-options-in-sifgrs/182.

Table 2.1. List of intragranular modeling options in Sifgrs and comparisons between the previous and the updated modeling option names. Default options are marked with * for UO_2 and with + for U_3Si_2. Models with a single options do not need ENUM names and are left blank.

Option	General Description	Fuel Type	Previous Integer	Updated ENUM Name	Option Description
`ig_fully_coupled`	Diffusion coupled to bubble evolution	All	0*	`LOOSELY_COUPLED`*	Loosely coupled
			1+	`FULLY_COUPLED`+	Fully coupled [8]
`ig_bubble_model`	Select bubble evolution model	UO_2	0*	`EMP_BAKER_WHITE`*	[30, 31]
			1	`FIXED`	Fixed bubble concentration and radius
			2	`NUCLEATION_RESOLUTION`	Bubble nucleation and re-solution
			3	`MECHANISTIC_AAGESEN`	For HBS [18]
		U_3Si_2	2+		Similar to case 3 for UO_2 [18]
`ig_diff_algorithm`	Select intragranular diffusion algorithm	All	0*	`FORMAS`*	Use Formas [5]
			1	`POLYPOLE1`	Use PolyPole1 [11]
			2+	`POLYPOLE2`+	Use PolyPole2 [8]
`ig_bubble_coarsening`	Enable intragranular bubble coarsening	All	0*,+	`NO_COARSENING`*,+	No coarsening
		UO_2	1	`WITH_COARSENING`	With coarsening [32, 9]

Table 2.2. List (part 1) of intragranular parameter options in Sifgrs and comparison between the previous and the updated parameter option names. Default options are marked with * for UO_2 and with + for U_3Si_2. Models without any other options do not need ENUM names and are left blank.

Option	General Description	Fuel Type	Previous Integer	Updated ENUM Name	Option Description
`eff_diff_coeff_option`	Select effective diffusion coefficient	All	0*	`INCLUDING_BUBBLE`*	Accounts for intragranular bubbles
		UO_2	1	`BULK`	No effects from bubbles
			2	`LASSMANN`	[6]
			99	`TEST_CASE`	Test case
`diff_coeff_option`	Select intragranular atomic diffusion coefficient	UO_2	0	`TURNBULL_D1_4D2`	Thermal D_1 and irradiation-enhanced $4D_2$ diffusion [33, 34]
			1	`ANDERSSON`	[14]
			2	`TURNBULL_D1_D2_D3`	Thermal D_1 and irradiation-enhanced $D_2 + D_3$ diffusion [33]
			3*	`TURNBULL_D1_D2`*	Thermal D_1 and irradiation-enhanced D_2 diffusion [33]
			4	`TURNBULL_D1_4D2_4D3`	Thermal D_1 and irradiation-enhanced $4D_2 + 4D_3$ diffusion [33, 34]
			5	`TURNBULL_D1_4D2_D3`	Thermal D_1 and irradiation-enhanced $4D_2 + D_3$ diffusion [33, 34]
		U_3Si_2	0	`U_VACANCY`	U vacancy self-diffusion [15]
			1	`U_VACANCY_ANISOTROPY`	Same, with anisotropy [15]
			2	`U_VACANCY_BARANI`	U-vacancy self-diffusion [10]
			3+	`SI_VACANCY_STOICHIOMETRY`+	Si-vacancy for stoichiometric U3Si2
			4	`SI_VACANCY_RICH`	Si-vacancy for Si-rich U3Si2
		All	99	`TEST_CASE`	Test case
	Select intragranular vacancy diffusion coefficient	UO_2	0*		Athermal [29]
		U_3Si_2	0	`U_VACANCY`	U vacancy self-diffusion [15]
			1	`U_VACANCY_ANISOTROPY`	Same, with anisotropy [15]
			2	`U_VACANCY_BARANI`	U-vacancy self-diffusion [10]
			3+	`SI_VACANCY_STOICHIOMETRY`+	Si-vacancy for stoichiometric U3Si2
			4	`SI_VACANCY_RICH`	Si-vacancy for Si-rich U3Si2
			99	`TEST_CASE`	Test case

Table 2.3. List (part 2) of intragranular parameter options in Sifgrs and comparison between the previous and the updated parameter option names. Default options are marked with * for UO_2 and with + for U_3Si_2. Models without any other options do not need ENUM names and are left blank.

Option	General Description	Fuel Type	Previous Integer	Updated ENUM Name	Option Description
res_param_option	Select resolution parameter	UO_2	0*	HETEROGENEOUS_WHITE*	Heterogenous [31]
			1	HOMOGENEOUS_LOSONEN	Homogenous, constant rate [35]
			2	HOMOGENEOUS_PASTORE	Homogenous, constant rate [7]
			3	HETEROGENEOUS_VESHCHUNOV	Heterogenous [36]
			4	HETEROGENEOUS_SETYAWAN	Heterogenous [32]
		U_3Si_2	0*	HOMOGENEOUS_MATTHEWS*	Constant re-solution parameter [37]
			1	HETEROGENEOUS_MATTHEWS	Depends on bubble radius [37]
		All	99	TEST_CASE	Test case
trap_param_option	Select trapping parameter	All	0*	DEFAULT*	Accounts for sink strength and size
			99	TEST_CASE	Test case
nucleation_option	Intragranular bubble nucleation model	UO_2	0*	HETEROGENEOUS*	Heterogeneous nucleation [38, 39, 30, 40]
			1	HOMOGENEOUS	Homogeneous nucleation [41, 42, 38]
		U_3Si_2	0*	HOMOGENEOUS*	Homogeneous nucleation [41, 42, 38]
		All	99	TEST_CASE*	Test case
doping_type	Select trapping parameter	UO_2	0*	UNDOPED*	Undoped UO2
			1	CR2O3_DOPED	Cr_2O_3-doped UO2
cr_doped_option	Select cromium (Cr)-doped option	UO_2	0	CORRECTION	Correction for $T \geq 1825$ K. Iteration for [43]
			1	TRANSITION_TEMPERATURE_1525	Temperature transition $T = 1525$ K. Iteration for [43]
			2	TRANSITION_TEMPERATURE_1800	Temperature transition $T = 1800$ K. Iteration for [43]
			3	TRANSITION_TEMPERATURE_1673	Temperature transition $T = 1673$ K. Iteration for [43]
			4	REFINED_1673	Temperature transition $T = 1673$ K, refined. Iteration for [43]
			5*	BEST_ESTIMATE_1773*	Best estimate, temperature transition $T = 1773$ K [43]
			6	UPPER_LIMIT_1773	Upper limit, temperature transition $T = 1773$ [43]

Table 2.4. List of transient model options in Sifgrs and comparison between the previous and the updated option names. These models are only available for UO_2, and the default option is marked with *.

Option	General Description	Fuel Type	Previous Integer	Updated ENUM Name	Option Description
transient_option	Select transient release model	All	0*	NO_TRANSIENT*	No Transient
		UO_2	1	MICROCRACKING_BURNUP	Microcracking, with burnup [13]
			2	MICROCRACKING	Microcracking, no burnup [13]
			3	EMPIRICAL_CAPPS	Empirical transient (to be added) [21]
			4	PULVERIZATION	Pulverization (to be added) [18]

2.3.9 Introduction of a data structure to limit code duplication between NR and HBS fuel

To prepare the extension of Sifgrs to HBS fuel (see Chapter 3), a data structure was developed to contain all the properties that would otherwise need to be duplicated for HBS fission gas modeling (i.e., amount of fission gas in the matrix, in intragranular bubbles, and in intergranular bubbles, the size and concentration of bubbles, the dislocation density, etc). This general data structure is general enough to be applied to NR fuel, the HBS fuel, and the complete fuel separately, and Sifgrs methods (i.e., functions for fission gas generation, intragranular diffusion, etc.) are now applied the general data structure rather than specific NR or HBS properties. As a result, these methods are more general and do not need to be duplicated for each fuel zone (NR or HBS). Using a data structure provides reusability, modularity, and ensures mass conservation between NR and HBS fuel.

2.3.10 Summary of Sifgrs refactoring efforts

This FY, the implementation of the Sifgrs model was profoundly refactored to meet the growing needs for HBS modeling and other fuel forms. The refactoring efforts described above have met the goals listed in Section 2.1 for modularity, robustness, and documentation. Although the impact of this effort cannot be directly measured, these changes have already enabled the rapid development of new Sifgrs capabilities (see HBS fission gas model described in Section 3.2 and UN Sifgrs development in Ref. [26]). Thanks to the designed modularity, the future development of fission gas capabilities will be greatly accelerated. However, as future needs evolve and grow in unexpected ways, attention should be paid to ensure that the Sifgrs implementation remains flexible and modular.

2.4 Model Implementation Corrections and Debugging

2.4.1 Prevent divisions by 0 in PolyPole2

In certain conditions, the quantity `p_pole` used in `PolyPole2` —the first term of the diagonal of $\mathbf{P}_n$ in Eq. (15) in Ref. [8]—could become equal to 0, which would lead to divisions by 0 later in `PolyPole2`. As a result, Sifgrs would be unable to predict fission gas behavior since several quantities (e.g., gas concentration in intragranular bubbles) would be undefined. To prevent this unwanted behavior, ‖`p_pole`‖ cannot be defined smaller than 1×10^{-20}. This makes Sifgrs significantly more robust for users.

2.4.2 Update for bubble resolution model under no fission rate

When quasi-steady state is assumed (i.e., when using `Formas` or `PolyPole1`), the amount of fission gas present in intragranular bubbles is determined using the ratio of trapping rate over the resolution rate. However, when the fission rate is null, then the resolution rate is null, as the only mechanism for fission gases to leave the bubbles is to be knocked out by a fission event [31, 32, 35, 7, 36]. To avoid dividing by 0, a special case had been implemented that effectively removed all the fission products from the bubbles when the fission rate reached 0. However, this approach is not physical and was leading to non-conservation of the total amount of fission gas in the system. Instead, all the fission gas is now assumed to be trapped in intragranular bubbles, as no resolution mechanism is active. This change results in physical

predictions and Sifgrs now conserves the amount of fission gas in the system as fission rate goes to 0. Figure 2.4 shows a new test using PolyPole1 that was added to BISON with a fission rate that decreases until becoming null and increases again. The amount of fission gas in the matrix and in the bubbles are tracked. Both previous and new results are shown, which shows the improvement resulting from this update as mass conservation is now ensured. The tests are called

- `formas_intragranular_intermediate_no_fission_rate`,
- `polypole1_intragranular_intermediate_no_fission_rate`,
- `polypole2_intragranular_intermediate_no_fission_rate`.

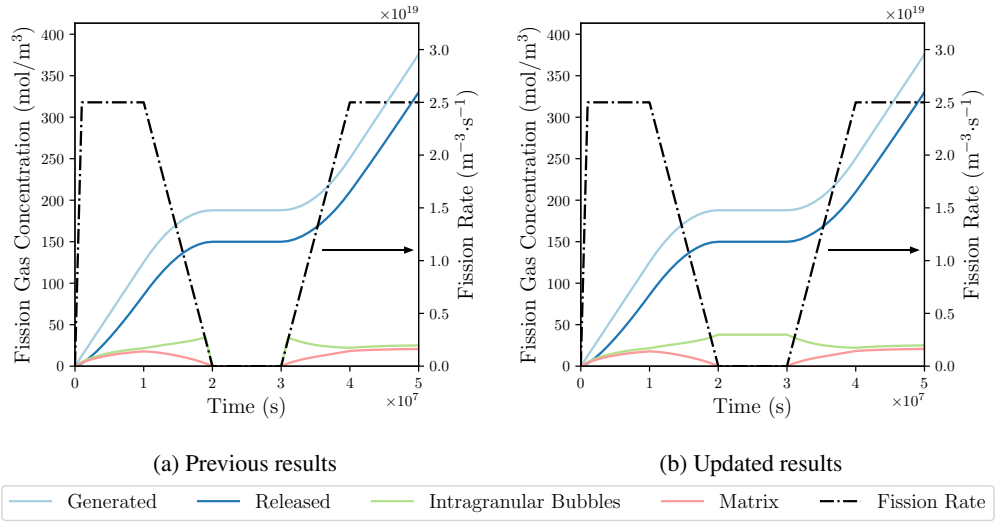

Figure 2.4. Comparison of the (a) previous and (b) updated model predictions for gas concentration in intragranular bubbles when the fission rate goes to 0. Updated results conserve the amount of fission gas in the system by maintaining the gas concentration in intragranular bubbles.

Moreover, a new test was added to assess the model behavior when the updated model for gas concentration in intragranular bubbles was coupled with the model of bubble evolution. In this test, the fission rate also goes to 0 and increases back up to test mass conservation. The new tests are called

- `formas_intragranular_bubble_evolution_intermediate_no_fission_rate`,
- `polypole1_intragranular_bubble_evolution_intermediate_no_fission_rate`,
- `polypole2_intragranular_bubble_evolution_intermediate_no_fission_rate`,

and the results when using PolyPole1 are shown in Fig. 2.5. The updated implementation avoids the sharp discontinuities in bubble concentration and radius predicted by the previous implementation. Moreover, fuel swelling is directly affected by these updates. The previous implementation underestimated the amount of intragranular swelling as the average intragranular bubble radius decreased significantly as the fission gas artificially disappeared.

Note that accurately predicting fission gas behavior as the fission rate goes to 0 is crucial. Indeed, it is necessary to compare PIE results to model predictions at the end of the irradiation history once the fuel is taken out of the irradiation conditions. Moreover, the previous implementation was not appropriate to model many of the LOCA tests performed experimentally under no irradiation, since a large amount of fission gas was not accounted for. The current implementation solves these issues.

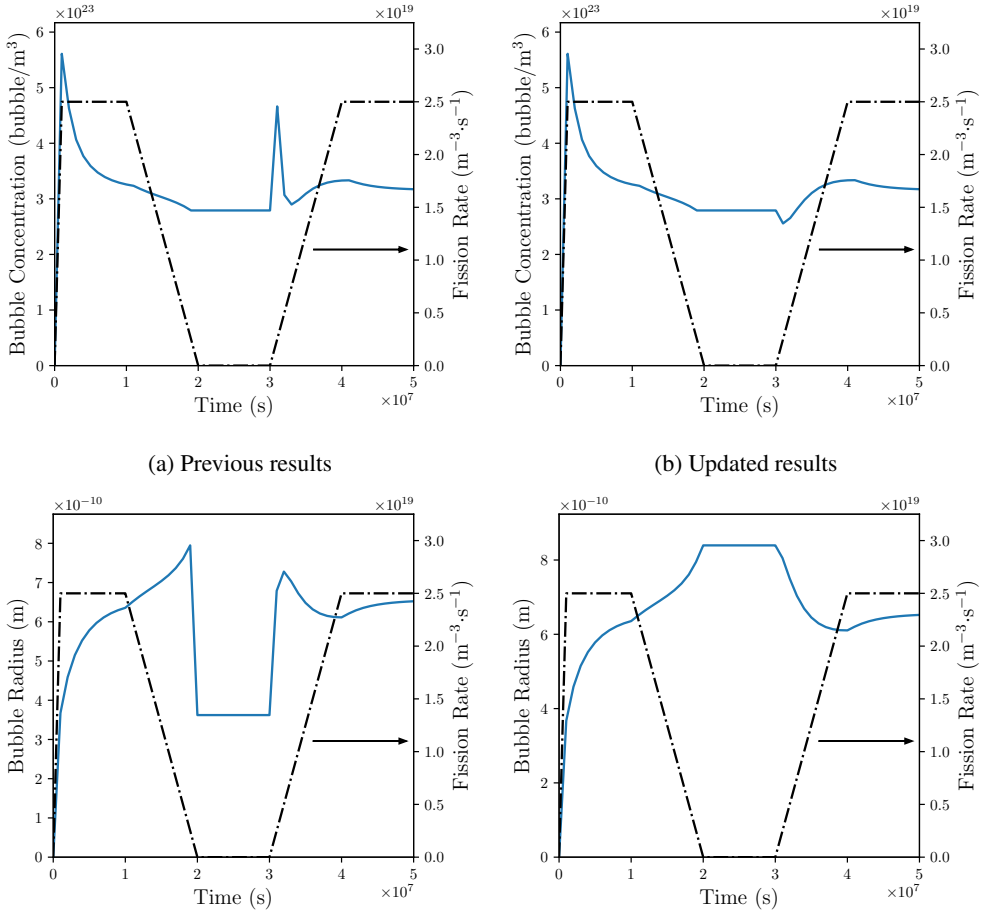

(a) Previous results

(b) Updated results

(c) Previous results

(d) Updated results

Figure 2.5. Results of a new test with the updated models for gas concentration in intragranular bubbles coupled with the bubble evolution model when the fission rate goes to 0. (a, b) show the changes in bubble concentration predictions; (c, d) show the changes in bubble radius predictions.

2.4.3 Update to the intragranular bubble coarsening model

Similarly to the bubble resolution model implementation issue described in Section 2.4.2, the implementation of the resolution model for bubbles pinned at dislocations was defective. As the fission rate became null, the amount of fission gas in the system was not conserved. Gas concentrations in intragranular bubbles and in bubbles pinned to dislocations could become several times greater than the amount of generated fission gas, providing unphysical results. The case with fission rate at 0 was corrected and Sifgrs now provide more physical predictions. Figure 2.6 shows a new test using PolyPole1 that was added to BISON with a fission rate that decreases until becoming null and increases again. The amount of fission gas in the matrix and in the bubble populations is tracked. Both previous and new results are compared, which shows the improvement resulting from this update as mass conservation is now ensured. The new tests are called `formas_intragranular_coarsening_intermediate_no_fission_rate` and `polypole1_intragranular_coarsening_intermediate_no_fission_rate`. Note that despite the significant improvement, the discontinuity in gas concentration in the two bubble populations as the fission rate reaches 0 might still need correction for the behavior to be fully physical.

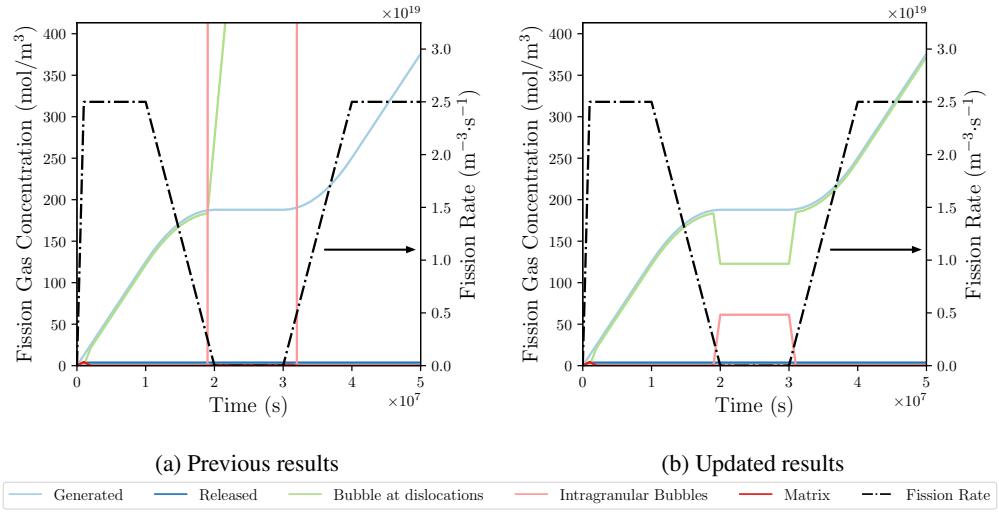

Figure 2.6. Results of a new test with the updated models for gas concentration in intragranular bubbles and bubbles at dislocations when using the coarsening model when the fission rate goes to 0. The updated implementation ensures mass conservation.

2.4.4 Update for Lassmann's HBS model implementation

The implementation of the model from Ref. [28] was found to be defective and did not reproduce the results presented in the original paper. The model assumes that HBS formation is immediate when the local burnup reaches a threshold value between 60 GWd/tU and 75 GWd/tU (or MWd/kgU). When the HBS forms, the model describes how the xenon (Xe) gas previously present in the grain interior (i.e., matrix) goes to HBS pores. Figure 2.7 shows the comparison between the test results of the previous implementation, the updated implementation, and the experimental

data and model presented in Ref. [28] when using polypole1 with an HBS threshold value of 70 MWd/kgU. The new implementation better matches the results presented in the original paper [28]. The new and updated tests are called `formas_intergranular_hbs`, `polypole1_intergranular_hbs`, and `polypole2_intergranular_hbs`. More information about the updated implementation is available in Section 3.2.3.1.

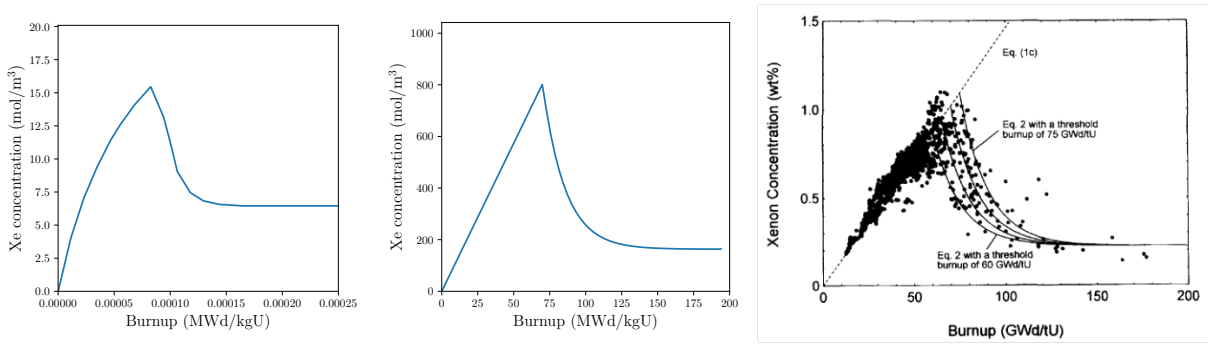

(a) Previous results (b) Updated results (c) Data from Ref. [28]

Figure 2.7. Comparison of the (a) previous (b) updated model predictions and (c) data and model predictions directly from Ref. [28] for HBS formation and gas transfer from grain interior to HBS pores. These simulations use polypole1 with an HBS threshold value of 70 MWd/kgU. The updated implementation better matches the data and model from Ref. [28], especially when considering the different orders of magnitude in burnup and xenon concentration between (a) and (b).

2.4.5 Issue when accounting for fission gases in HBS with `UO2PulverizationMesoscale`'s model

As mentioned in Section 2.3.7, the amount of generated fission gas was counted twice when `UO2PulverizationMesoscale` was used—both in low-burnup and HBS fuel. In addition, since `UO2PulverizationMesoscale` had not been coupled with Sifgrs, it initialized the bubble pressure with a fixed value independent of previous history. As such, the initial gas concentration in HBS bubbles could be greater than the total amount of generated fission gas. These implementation choices resulted in an overestimation of fission gases where HBS formed. Fig. 2.8 shows the predictions made by the previous Sifgrs and `UO2PulverizationMesoscale` implementation, which used an adapted version of Barani's model for HBS formation [9]. Fission gases are not conserved, as the total amount of fission gases is significantly greater than the amount of generated fission gases. To fix this issue, Sifgrs had to be significantly modified to enable the proper modeling of fission gases in HBS, which requires modeling of gas generation, transfer from low burnup to HBu fuel, and gas behavior within the HBS. These changes are the focus of Section 3.2.

2.4.6 Update to enable recover with Sifgrs

The restart and recover system in Multiphysics Object-Oriented Simulation Environment (MOOSE) enables the checkpointing of state in a simulation and the use of these checkpoints to "restart" the simulation at a later time. A common

use case is the continuation of a HPC job that has run past its allowed simulation time, where the job was completely killed.

There was a significant bug within Sifgrs that restricted it from loading the proper state within a restart. This bug was not noticed until a recent change to MOOSE that simplified the restart system and exposed cases where the state was loaded incorrectly within an API call. In particular, it was enforced that only stateful material properties are loaded within the `Material::initStatefulQpProperties` API. Within Sifgrs, the variable `_nmodes_polypol2_max` (which is not a stateful material property) was initialized within said API.

The correction for this specific bug was to properly initialize `_nmodes_polypol2_max`, which is now done at construction time. This fix enables restarting simulations using Polypole2, which is currently the most sophisticated algorithm used in BISON to resolve intragranular fission gas distribution [8].

2.5 Summary

Sifgrs was refactored this FY to address the growing need to expend its capabilities to new fuel forms (e.g., UN) and new conditions (e.g., HBu conditions). As such, we increased the amount and quality of tests, we made major changes to the code structure to make it more modular and decrease code duplication, and we increased documentation and made the code more user friendly. During that process, capabilities were maintained or improved if errors and bugs were identified.

The updated implementation of Sifgrs enabled the quick and efficient development of fission gas release and

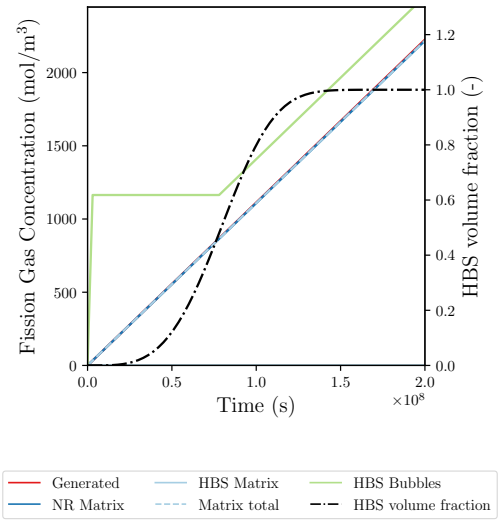

Figure 2.8. Previous predictions from Sifgrs and `UO2PulverizationMesoscale`. Fission gases are not conserved, with the gas concentration in HBS bubbles greater than the concentration of total generated gas. This is due to the fact that fission gas calculations within HBS are independent and therefore duplicates of calculations in Sifgrs. Improvements are described in Section 3.2.

swelling capabilities for UN fuel [26] and the addition of HBS capabilities, which is described in Chapter 3. This new implementation was designed to remain modular and flexible for identified future modeling needs. The current effort should therefore greatly reduce the resources needed to implement new capabilities to Sifgrs in the future. However, it is important to note that as with every other model implementation, the code structure should continue to be updated as needs evolve.

3. MODEL DEVELOPMENT IN Sifgrs FOR HBS AND tFGR MODELING

As the nuclear industry's desire to extend burnup beyond current licensing practices grows to optimize fuel utilization, the need to understand HBu fuel performance becomes urgent. At HBu, new mechanisms of FGR emerge, leading to an important increase in FGR that cannot be explained with the low-burnup fuel models [21, 44, 45, 46, 47, 1]. Several experimental programs exhibited a large increase in FGR during transients [44, 45, 46, 47]. This contribution, called tFGR, becomes increasingly significant with increasing burnup and may impact the ballooning and burst behavior of HBu fuel [1, 48]. These experimental programs also concluded that tFGR originates from intergranular bubbles, and tFGR is a result of (1) important microstructural changes—including HBS and dark zone formation [20] and bubble interconnection—and (2) fuel pulverization, which led to the release of the gas located in overpressurized bubbles. These experimental results highlight the complexity of the phenomenon and the need for a better understanding of the governing mechanisms to appropriately address associated risks.

In this report, we first present an empirical model developed in Ref. [21]. The model highlights the dependence of tFGR on temperature and burnup for single pellet experiments from the GASPARD program but does not perform as well in other conditions. The limitation of such an empirical model emphasizes the need for a mechanistic HBu tFGR model. In the rest of the section, we present recent development toward that goal. The mechanistic model describes the HBS formation, the fission gas transport from the NR to the HBS region, the intragranular and intergranular fission gas behavior, the pulverization of the HBS structure, and the resulting tFGR.

3.1 Empirical Model for tFGR

3.1.1 Context for the development of the empirical tFGR model

As described above, tFGR is not well understood, even empirically, and only limited data is available. To alleviate these challenges, a paper has been written as a collaboration between the NEAMS and Advanced Fuels Campaign (AFC) programs to summarize the publicly available tFGR data, discuss the observed dependencies (e.g., burnup, heating rate, sample geometry, and terminal temperature), and propose an empirical model for tFGR [21]. In this report, we recall parts of Ref. [21] that are directly relevant to the current work. More information is available in the paper [21].

3.1.2 Model description

Table 1 and Fig. 1 from Ref. [21] summarises the available experimental tFGR data from fuel sample and fuel pellet heating tests, which originates from Refs. [49, 50, 51, 47, 52]. It also emphasizes the impact of hydrostatic pressure, heating rate dependencies, and terminal temperature on tFGR as a function of burnup.

The empirical transient model is a function of local burnup and temperature. Details of the development of the model and the fitting process can be found in Ref. [21]. The equation for transient fission gas release can be written as a function of burnup β and temperature T

$$FGR(T,\beta) = \frac{100 - \frac{\beta^2}{f}a_2}{\left(1 + e^{-\frac{T-x_0}{\beta b_1}}\right)^c} + \frac{\frac{\beta^2}{f}a_2}{\left(1 + e^{-\frac{T-x_2}{b_2}}\right)^{c_2}}, \tag{3.1}$$

where FGR is the percent of fission gas release. The constants associated with the model are included in Table 3.1. Note, however, that the expression and parameter values do not exactly match the model described in Ref. [21] to represent recent updates to the model. Ref. [21] shows the GASPARD experimental data on which the model was fitted along with the model performance.

Table 3.1. Parameter values for the fitted empirical tFGR model presented in Eq. (3.1).

Parameter	Value	Units
f	65.320	$\frac{GWd^2}{tU^2}$
a_2	0.03552	(-)
x_0	1827.0	K
b_1	0.4077	$\frac{K^2 tU}{GWd \cdot min}$
c	0.2010	(-)
x_2	928.90	K
b_2	20.650	$\frac{K^2}{min}$
c_2	0.2230	(-)

3.1.3 Results

The model was validated using data from the GASPARD program, and its predictions are shown in Fig. 3.1. The model performs well in conditions similar to its training data.

3.1.4 Limitations and need for a mechanistic model

However, this empirical model is limited to conditions for which fitting data exist. As shown in Fig. 3.2, the model does not perform adequately when applied to conditions used by Noirot et al. [50].

Therefore, a high-level discussion is included in Ref. [21] to provide a roadmap for atomistically informed multiscale modeling in conjunction with an experimental data collection to develop a mechanistic tFGR model widely

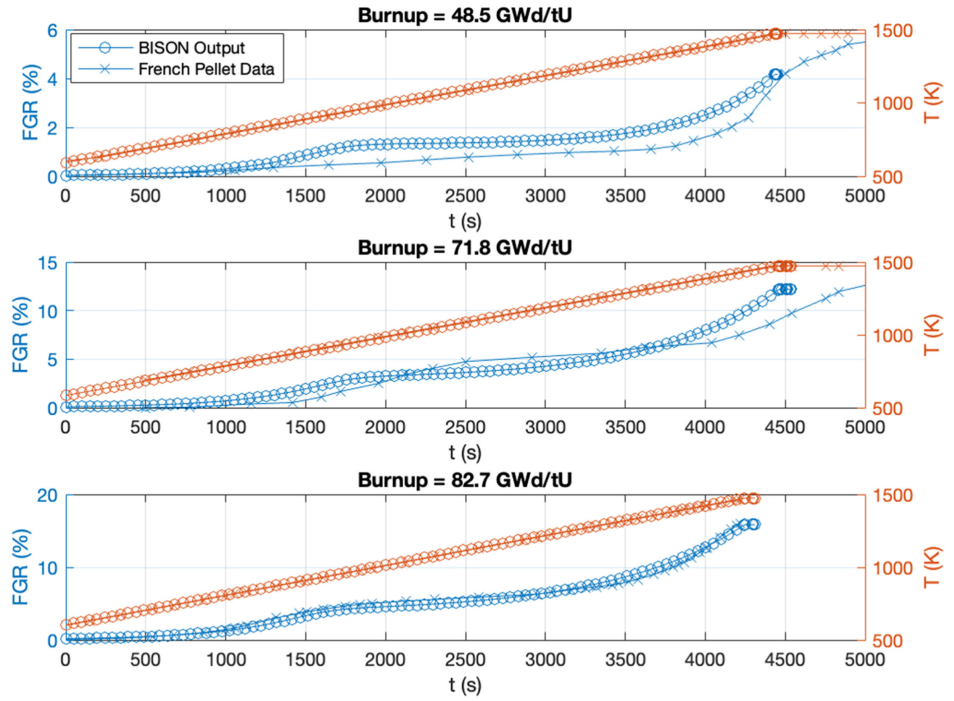

Figure 3.1. BISON prediction of FGR compared with the standard single-pellet data from the GASPARD program during thermal transient. Blue circles represent the BISON output at the temperatures (red circles), and blue crosses represent the experimental data for four burnup conditions. This figure is taken from Ref. [21].

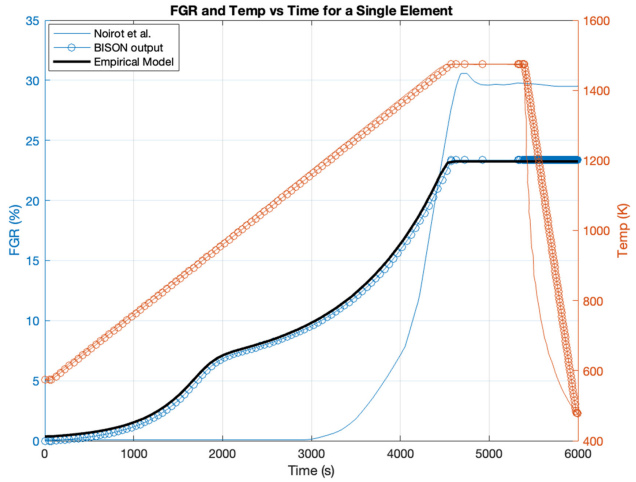

Figure 3.2. BISON prediction of FGR compared with a HBu experiment performed in Noirot et al. [50] during thermal anneal. Blue circles represent the BISON output at the temperatures denoted by the red circles, blue solid lines represent the experimental FGR, and red solid lines represent the temperature data. The predictive capabilities of the empirical tFGR model are limited in conditions outside of its training data. This figure is taken from Ref. [21].

applicable to a broad range of nuclear fuel conditions at HBu. This roadmap is summarized in Fig. 3.3. The remainder of this section focuses on developing some of the required capabilities at the engineering scale with insight from lower length scales.

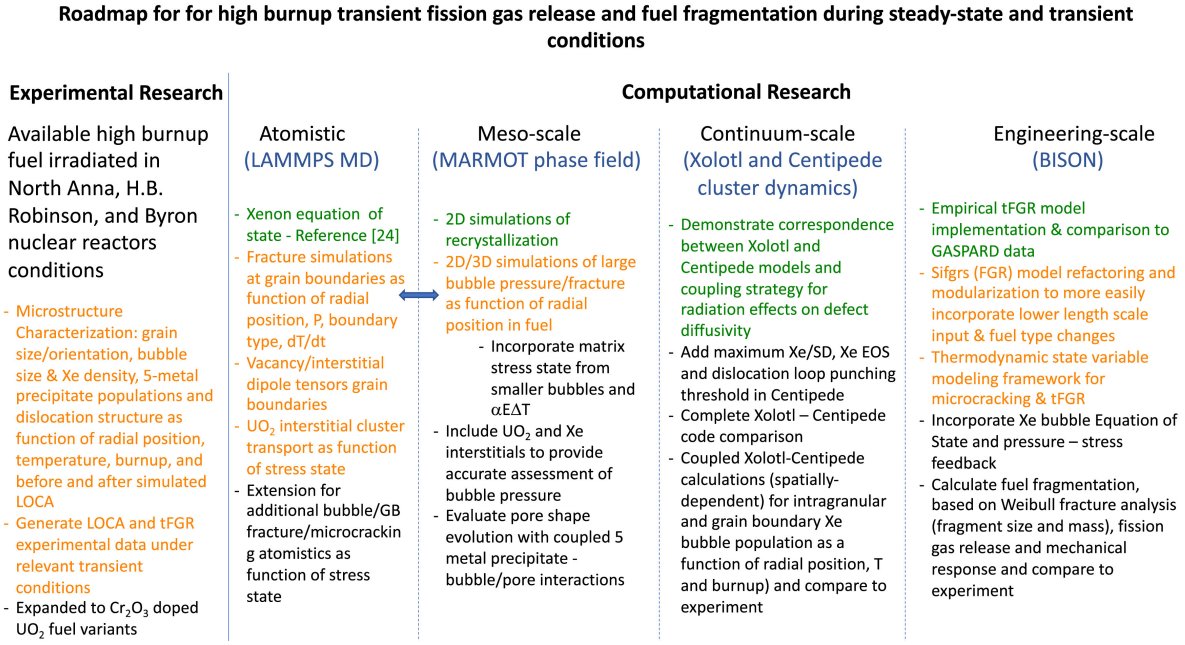

Figure 3.3. Roadmap of ongoing and planned experimental and computational research activities (green = completed, orange = ongoing, and black = future work) to improve knowledge and modeling capability for HBu transient fission gas release and fuel fragmentation during steady-state and transient conditions. This figure is taken from Ref. [21].

3.2 Modeling Fission Gas Behavior in HBS with Sifgrs

3.2.1 Modeling of HBS formation

As discussed in Section 2.3.7, several models are available in BISON for HBS formation, and these can be directly used in parallel with Sifgrs. Although many models exist in the literature, BISON currently offers two HBS formation models. The first one is an empirical description from Lassmann et al. [28], which was mentioned in Section 2.4.4. Barani et al. later developed a more descriptive model for HBS formation [16].

3.2.1.1 HBS formation model from Lassmann et al.

The model from Lassmann et al. assumes that all the fuel transforms to HBS once the local burnup reaches a given threshold bu_0 (70 MWd/kgU). It also describes the fission gas transition from NR to HBS fuel, which will be described in Section 3.2.3.1.

3.2.1.2 HBS formation model from Barani et al.

Barani's model uses the local effective burnup bu_{eff} from Ref. [53]—as opposed to the local burnup bu—to predict HBS formation [16]. The local effective burnup is defined as

$$bu_{eff} = \int f(T - \bar{T}) d\, bu \tag{3.2}$$

where f is the Heaviside step function, T the local temperature in Kelvin, and $\bar{T} = 1000°\,\mathrm{C} = 1273.15\,\mathrm{K}$ is a threshold temperature in Kelvin. The volume fraction of restructured fuel α is then derived using an adapted version of the JMAK model [54]:

$$\alpha = 1 - \exp\left(-K\, bu_{eff}^{\gamma}\right) \tag{3.3}$$

where $K = 1.52{\times}10^{-7}$ (MWd/kgU)$^{-\gamma}$ is the transformation rate constant, and $\gamma = 3.54$ (-) is the Avrami constant. Note that the parameter values are slightly different than what is published in Ref. [16] to account for the latest developments.

Barani's model will be used in this work due to its ability to predict local partial HBS formation and its performance when predicting the experimental measurements from Refs. [55, 56] and others (see [16]).

Although Barani's model appropriately predicts HBS formation at the rim region, it does not predict the fuel restructuring deeper in the fuel pellet observed experimentally [20]. Future work is needed to fully model fuel restructuring.

3.2.2 A two phase model for the non-restructured region and HBS

As in Barani's model [16], the fuel is modeled as a two-phase system, with the fuel being part non-restructured and part HBS. Fission gas concentration is therefore shared between the two phases, with

$$c^{tot} = (1 - \alpha) c^{NR} + \alpha c^{HBS}, \tag{3.4}$$

where c^{tot} (mol/m^3) is the local fission gas concentration, c^{NR} (mol/m^3) is the local fission gas concentration in the non-restructured (NR) phase, and c^{HBS} (mol/m^3) is the local fission gas concentration in the HBS phase. α is the local fraction of HBS provided by Eq. (3.3). Moreover, the grain size, bubble populations, dislocation density, and other microstructure parameters of each phase are tracked for each phase and for the complete fuel. This approach is similar to what is implemented in SCIANTIX [16] and MARGARET [57].

Note that the same description is used with Lassmann's model. However, as the local HBS volume fraction is either 0 or 1 (see Section 3.2.1.1), the two phase description is greatly simplified.

3.2.3 Modeling of fission gas transition from the non-restructured region to HBS

3.2.3.1 Lassmann's model

It has been observed experimentally that the gas within the matrix (intragranular gas) is gradually depleted as the HBS forms [28]. This depletion has been fit empirically with an exponential function that is valid when the current burnup

bu is greater than a threshold burnup bu_0. Lassmann et al. describe it as

$$c_{Xe}^{m} = \dot{s}_{Xe}\left[\frac{1}{a} + \left(bu_0 - \frac{1}{a}\right)e^{-a(bu-bu_0)}\right] \tag{3.5}$$

where c_{Xe}^{m} is the Xe concentration in the matrix, $\dot{s}_{Xe}$ is the Xe production rate, and $a = 5.84 \times 10^{-2}$ (MWd/kgU)$^{-1}$ is a constant fit to data. Once $bu > bu_0$ and depletion of the intragranular gas begins, it is assumed that the intragranular gas is transferred to the large intergranular bubbles normally observed in the HBS region at a rate proportional to concentration, following

$$\frac{dc_{Xe}^{m}}{dbu} = -ac_{Xe}^{m}, \tag{3.6}$$

$$\frac{dc_{Xe}^{HBS}}{dbu} = ac_{Xe}^{m}, \tag{3.7}$$

where c_{Xe}^{HBS} is the concentration throughout the fuel of Xe that is contained in HBS bubbles (to be distinguished from the concentration of Xe in each bubble, c_{Xe}^{b} which is significantly higher). This expression for rate of transfer, combined with the source term for production of new Xe atoms, can be integrated to obtain Eq. (3.5) [28]. As described in Section 2.4.4, the model was not properly implemented in Sifgrs. The new implementation of the model has been validated, and the results are shown in Fig. 3.4.

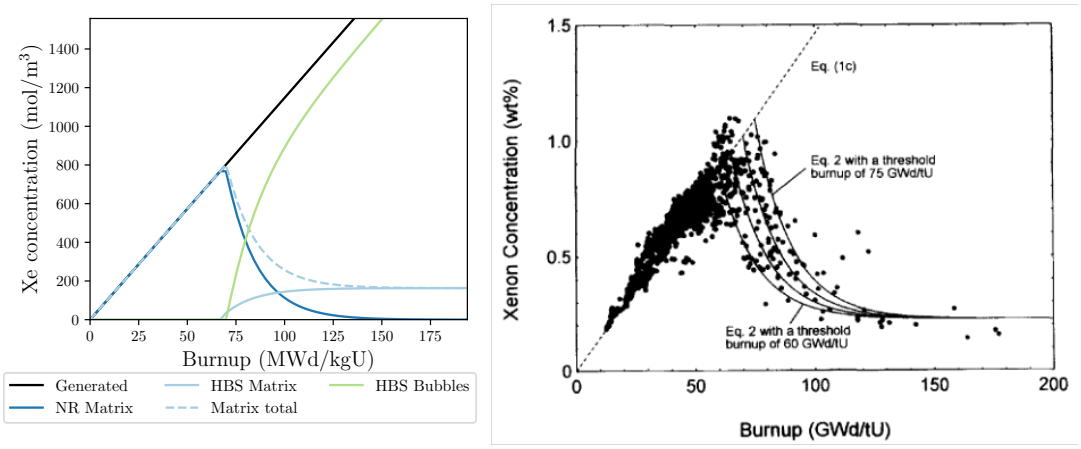

(a) Updated model implementation

(b) Data from Ref. [28]

Figure 3.4. Comparison of the (a) latest Lassmann model implementation and (b) data and model predictions directly from Ref. [28] for HBS formation and gas transfer from grain interior to HBS pores. The simulation uses PolyPole2 with an HBS threshold value of 70 MWd/kgU. The updated implementation matches the data and model from Ref. [28] and accounts for the distribution of fission gases in NR and HBS matrix.

3.2.3.2 An adaptation of Barani's model

As the fuel transitions to HBS, significant microstructural changes happen (e.g., subgrain formation and appearance of large pores). These transformations result in significant changes in the location of fission gases. As HBS forms during

irradiation, fission gases are swept from the non-restructured region. As the HBS volume fraction increases by $\Delta\alpha$, the amount of fission gas swept from the non-restructured region corresponds to

$$\Delta c^{NR} = -\frac{\Delta\alpha}{1-\alpha} c^{NR}. \tag{3.8}$$

The denominator $1-\alpha$ corresponds to the volume fraction of non-restructured fuel. In this model, we assume that the generation of fission products has already been accounted for, so mass conservation imposes that the amount of fission gas swept from the non-restructured fuel equals the amount of fission gas added to the HBS phase. As such,

$$\Delta c^{HBS} = -\Delta c^{NR}. \tag{3.9}$$

Once implemented into Sifgrs, or more precisely into `UO2Sifgrs`, it fixes the mass conservation issue raised in Section 2.4.5. The updated results are shown in Fig. 3.5c. As HBS formation happens, the amount of fission gases in the non-restructured matrix decreases. As all the fuel becomes covered by HBS, all the fission gases are located in the HBS phase. Note that in this simulation, diffusion of fission gases from HBS matrix to HBS bubbles is assumed to be instantaneous.

3.2.4 Intragranular fission gas modeling in HBS

As a first approximation, the intragranular fission gas behavior in HBS fuel is greatly simplified. HBS grains are assumed to have a constant radius of 150 nm [16], and intragranular fission gases are assumed to diffuse toward grain boundaries. The presence of intragranular bubbles and dislocations, which can affect fission gas transport in non-restructured fuel, are neglected. This assumption, however, is reasonable as a first approximation. HBS formation has been observed to reduce the density of dislocations, and the HBS microstructure is dominated by large intergranular bubbles rather than intragranular ones. Moreover, the purely diffusional description of intragranular fission gas behavior is widely used in fuel performance codes [16]. In the current report, we use the same diffusion coefficient as proposed in [16], which originates from an empirical study [58]. The diffusion of gas atoms in intragranular HBS is therefore defined as

$$D^{HBS} = 4.5 \times 10^{-42} F, \tag{3.10}$$

where F the fission rate in $\mathrm{m^{-3}s^{-1}}$), leading to D^{HBS} being defined in $\mathrm{m^2/s}$. Modeling HBS intragranular diffusion rather than assuming that fission gases immediately reach HBS bubbles leads to the results shown in Fig. 3.5d. Fission gases are now shared between HBS matrix and bubbles. The amount of fission gases in the HBS matrix now reaches a non-zero value, which depends on HBS grain size and HBS intragranular diffusivity. This model will be validated in future work. In particular, it will be compared to the experimental data published in Ref. [28].

Note that when Lassmann's model of HBS formation is used, the sweeping of fission gases from the intragranular matrix to HBS bubbles already accounts for intragranular diffusion in the HBS region (see [28] and Section 3.2.3.1). As such, no further intragranular model is needed.

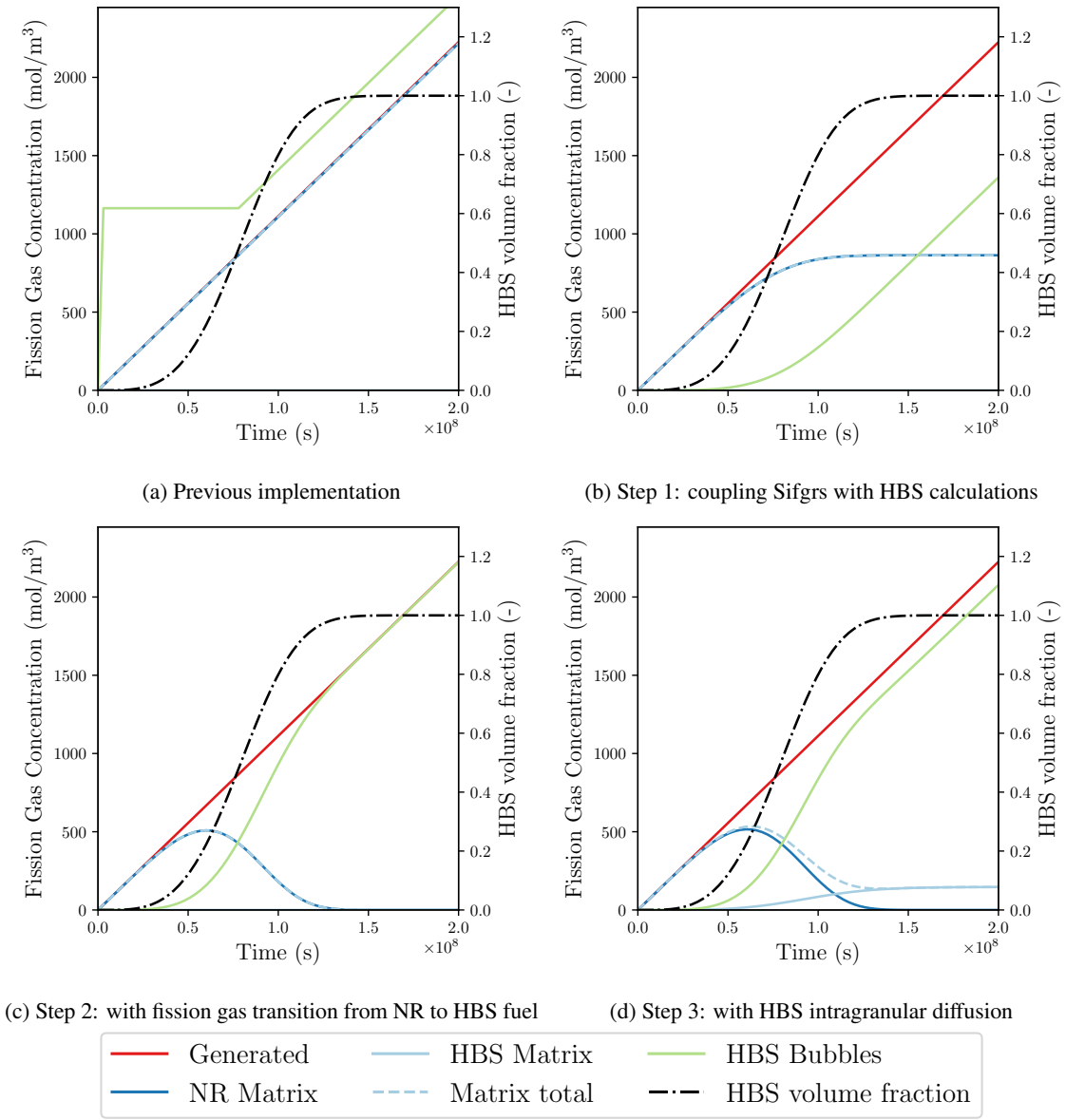

(a) Previous implementation

(b) Step 1: coupling Sifgrs with HBS calculations

(c) Step 2: with fission gas transition from NR to HBS fuel

(d) Step 3: with HBS intragranular diffusion

Figure 3.5. Evolution of fission gas behavior during HBS formation during the refactoring of Sifgrs and the implementation of the new model. (a) shows the original implementation, without mass conservation due to a disconnect between Sifgrs and HBS modeling. (b) shows the results once the HBS formation was coupled with Sifgrs, leading to mass conservation. (c) shows the results once fission gases were properly transferred from NR to HBS fuel, assuming that all fission gases present in the matrix immediately reached HBS bubbles. Finally, (d) shows the current implementation accounting for generation and diffusion in the HBS matrix based on Eq. (3.10).

3.2.5 Intergranular fission gas modeling in HBS

In the original BISON UO_2 pulverization model developed in FY-21 and FY-22, the fission gas behavior in HBS was disconnected from the low-burnup behavior. The pulverization model did not realistically track the gas concentration evolution in the surrounding fuel matrix or the evolution of intergranular bubbles as the HBS formed. Matrix gas concentration and intergranular bubble evolution are normally tracked by the Sifgrs model, and the pulverization model was not integrated with Sifgrs. Thus, the initial formation of the bubbles in the HBS region was not modeled in a physically realistic way, and the Sifgrs model continued to evolve the gas concentration evolution without accounting for HBS formation.

Now that Sifgrs has been refactored and that it became much more modular (see Chapter 2), the bubble evolution model for the HBS region has been revised and moved to Sifgrs so that the transition between pre-HBS and HBS bubble microstructures is captured more realistically (see Section 2.4.5). All material properties that were previously used in `UO2PulverizationMesoscale` to track the properties of the bubble microstructure in the HBS region have now been moved to `UO2Sifgrs`. This significantly improves the pulverization criterion and the Sifgrs model.

In FY-21, the initial pressure of the HBS bubbles was assumed to be 100 MPa at a temperature of 400°C [17], based on the dislocation punching criterion surrounding bubbles in the HBS region [59]. Phase-field simulations of the HBS formation process in the previous FY milestone showed dislocation punching pressure to be a reasonable estimate of the initial bubble pressure [17, 18]. The initial average bubble radius was assumed to be 0.53 μm [60], and it was assumed that the bubble size and pressure remained static after HBS formation. In FY-22, the model was modified to account for growth of the bubble size and change in bubble pressure based on gas atom production and overpressurization-driven vacancy flux, assuming the bubbles started from 100 MPa at a temperature of 400°C and radius 0.53 μm at the time of HBS formation [18]. In previous reports, preliminary models for fuel pulverization and tFGR have been developed to address this challenge [17, 18]. The models used lower length scale models to describe the pressurization of HBS bubbles, determine the critical bubble pressure, and provide a criteria for fuel pulverization and the resulting release of fission gases.

In addition to the intragranular gas described above, the transfer of intergranular gas contained in the grain boundary bubbles to the larger, spherical bubbles found in the HBS region must be accounted for. Moreover, it is assumed that gas is transformed from the intergranular bubbles to the HBS bubbles at the same rate as rate of formation of the HBS itself. Taking the derivative of Eq. (3.3) with respect to burnup gives the rate of change of volume fraction with respect to burnup:

$$\frac{d\alpha_{HBS}}{dbu} = \gamma K bu_{eff}^{\gamma-1} \exp\left(-K bu_{eff}^{3.54}\right). \tag{3.11}$$

Thus, the rate of change of grain boundary bubble density, N_{gb}, is given by

$$\frac{dN_{gb}}{dbu} = N_{gb}\frac{d\alpha_{HBS}}{dbu}. \tag{3.12}$$

Alternatively, we can just determine what N_{gb} is when we reach $bu = bu_{eff}$, and then reduce N_{gb} by Eq. (3.3).

Having determined how much gas is transferred to the HBS bubbles, we now must determine their pressure and size evolution. It is assumed that initial number density of HBS bubbles N_{HBS} is 2×10^{17} m^{-3} [10], and their initial radius

R_b is set to 0 μm. Note that gas bubbles in the HBS region are assumed to be spherical, in contrast to the lenticular intergranular (grain boundary) bubbles that are normally observed in UO_2 fuel prior to HBS formation. The density of gas in each bubble, c^b_{Xe}, is calculated by

$$c^b_{Xe} = \frac{c^{HBS}_{Xe}}{N_{HBS} V_b}, \tag{3.13}$$

where $V_b = \frac{4}{3}\pi R_b^3$ is the bubble volume. Now having determined the concentration of gas in each bubble, we can determine the bubble pressure P using the equation of state of our choice.

To evolve the bubble radius as a function of time, an approach similar to that used for the evolution of intragranular bubbles in U_3Si_2 [10, 61] was employed. The growth of the bubbles is assumed to be controlled by vacancy flux, driven by overpressurization of the HBS bubbles. It has been shown using atomistic calculations [62, 63, 64] that at the lower temperatures normally found in the rim of light-water reactor (LWR) UO_2 fuel ($T < 1200K$), interstitial Xe is the dominant mobile Xe species. Thus, adding Xe atoms to existing bubbles does not change the bubble volume, and bubble growth is controlled by vacancies only. Given this, the rate of change of bubble volume is given by

$$\frac{dV_b}{dt} = \Omega \frac{dn_{iv}}{dt}, \tag{3.14}$$

where $\Omega = 4.09 \times 10^{-29}$ m^3 is the volume of a U lattice site in UO_2 [23], and n_{iv} is the number of vacancies per intragranular bubble. For overpressured bubbles, the vacancy flux is given by [10, 61]:

$$\frac{dn_{iv}}{dt} = \frac{2\pi D^v_{ig} \rho}{kT\zeta} \left(P - P_{eq}\right), \tag{3.15}$$

where D^v_{ig} is the intragranular vacancy diffusion coefficient, ρ is the radius of the equivalent Wigner-Seitz cell surrounding a bubble, and ζ is a dimensionless factor defined as:

$$\zeta = \frac{10\psi(1+\psi^3)}{-\psi^6 + 5\psi^2 - 9\psi + 5}, \tag{3.16}$$

where $\psi = R_b/\rho$. P_{eq} is the equilibrium pressure for a bubble of radius R_b, as calculated using the Laplace-Young equation

$$P_{eq} = \frac{2\gamma}{R_b} - \sigma_h, \tag{3.17}$$

where $\gamma = 0.85$ J/m^2 [22, 23] is the surface tension of the bubble-matrix interface, and σ_h is the hydrostatic stress, considered to be negative for a solid in compression. Since the bubbles are expected to be overpressurized shortly after formation, we enforce $\frac{dn_{iv}}{dt} > 0$ to prevent transient bubble shrinking during the brief initial stage after bubble formation.

3.3 Updated Pulverization Criterion Based on 3-D Phase-field Fracture Results

3.3.1 Empirical pulverization model

An empirical criteria for fuel pulverization was first proposed in Refs. [65, 19]. It predicts fuel pulverization based on the local burnup and the local temperature, as shown in Fig. 3.6. This model is available in BISON as one of the options to predict fuel pulverization.

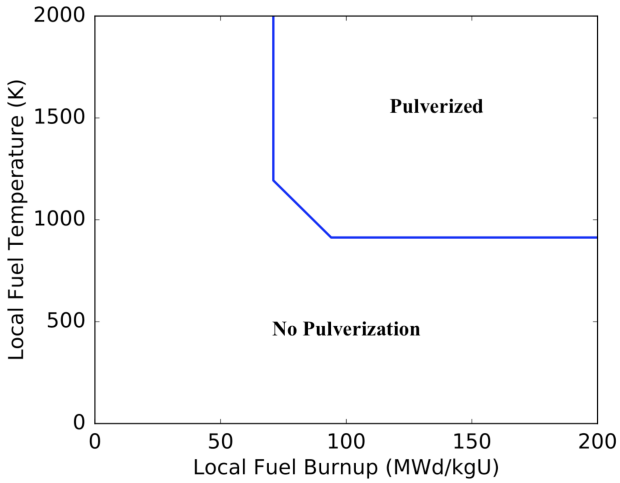

Figure 3.6. Empirical threshold for fuel pulverization [65, 19].

3.3.2 Mesoscale-informed pulverization model

The BISON pulverization criterion was updated last FY based on the bubble pressure obtained from the simplified 3-D phase-field fracture simulations [17, 18]. Here, the function for the critical bubble pressure is expressed as a function of porosity, critical fracture stress, and applied external pressure, such that

$$P_g^{cr} = [a + b\,(\sigma_{cr} - 130)](1 - c\,p) - d\,P_{ext}, \tag{3.18}$$

where σ_{cr}(MPa) is the critical fracture stress, p is the porosity, P_{ext}(MPa) is the external applied pressure, and a, b, c, and d are fitting coefficients. For the BISON pulverization criterion, the values of a, b, c, and d were obtained by fitting the data from lower length scale simulations using Python's `curve_fit` function. Thus, the fitted function of critical bubble pressure was:

$$P_g^{cr} = [175.987 + 0.5035(\sigma_{cr} - 130)](1 - 1.582p) + 1.089\,P_{ext}, \tag{3.19}$$

where pressures and stresses are provided in MPa. Comparisons of the fitted function and simulation data for a few select cases are shown in Ref. [17, 18]. The coefficient values were updated from the previous year's model, which was derived from the 2-D calculations. A linear trend was observed for all the input parameters. Note that this model also limits pulverization to the HBS region. The local volume fraction of HBS must be above a threshold value, which defaults to 0.5.

3.4 Modeling of tFGR from HBS

The mechanisms governing tFGR remain unclear. It is a complex phenomenon that depends on many variables (e.g., burnup, irradiation history, temperature history, fuel fragmentation, and hydrostatic pressure), and for which only a limited amount of experimental data is yet available. In this model, we focus on the potential contribution of pulverization of the outer rim of the fuel pellets on tFGR, which is estimated to correspond to 32–45% of fission gas [46, 47, 52]. We thus neglect other contributions (e.g., release from the central zone of the pellet, which is estimated to represent 22% of the fission gas [46, 47, 52]). The proposed mechanism relies on the sudden opening of many pores during fuel pulverization, thus releasing their fission gases. This model was first proposed last year in Ref. [18]. However, the model was disconnected from Sifgrs since it did not include the required HBS capabilities. Now that we refactored Sifgrs, we were able to directly couple low-burnup and HBu capabilities under a cohesive Sifgrs implementation, and the tFGR model is now coupled with Sifgrs. Sifgrs is now able to model low-burnup fission gas behavior, account for HBS formation, and describe HBS bubble growth, fuel pulverization, and the resulting tFGR.

We quickly summarize the tFGR below, but an exhaustive description is available in Ref. [18]. During fuel pulverization, a significant fraction of the HBS bubbles become exposed to free surfaces and release fission gas. The amount of FGR due to pulverization, n_{FG}^{pul}, is equal to

$$n_{FG}^{pul} = \frac{V_{b,open}^{pul} P_{FG}}{RT} = f_V^{pul} \frac{V_b^{pul} P_{FG}}{RT}, \tag{3.20}$$

where $V_{b,open}^{pul}$ is the volume of pores that become exposed during fragmentation, P_{FG} is the bubble pressure, R is the gas constant, and T is the temperature, V_b^{pul} is the bubble volume in pulverized fuel, and

$$f_V^{pul} = \frac{V_{b,open}^{pul}}{V_b^{pul}} = \frac{\sum_{bi} V_{bi,open}^{pul}}{\sum_{bi} V_{bi}^{pul}} \tag{3.21}$$

is the volume fraction of pores opened during fuel pulverization, with *bi* designating each HBS bubble. f_V^{pul} is expected to depend on pore structure, fragment size, and porosity, and this dependence has to be quantified.

To quantify how f_V^{pul}—and by extension n_{FG}^{pul}—depends on fragment size, pore size, and porosity, a Python script was written to automatically generate 3-D pore structures and determine the corresponding f_V^{pul}. Given a specific fragment size, bubble size, and porosity, the algorithm adds pores with the desired radius at random locations in and around a cube fragment until the desired porosity is reached. Each time a pore is added to the fragment, its contributions

to the total pore volume V_{bi}^{pul} and open pore volume $V_{bi,open}^{pul}$ are calculated. When the pore structure is created, its f_V^{pul} is derived. Note that two pores cannot be in contact with each other, and that even though bubbles can be partly outside the fragment, porosity calculations only include the pore volume that intersects with the fragment. Examples of generated pore structures at different porosity levels and different bubble sizes are shown in Fig. 3.7. The generated pore microstructure, although rudimentary, represents relevant porosity levels and pore/fragment sizes for HBS. The porosity levels therefore varied between 1 and 13% [66, 2, 61], the fragment size corresponds to tens of microns [49, 67], and bubble radii varies between 0.01 μm and 5 μm [68, 49, 67, 69, 52].

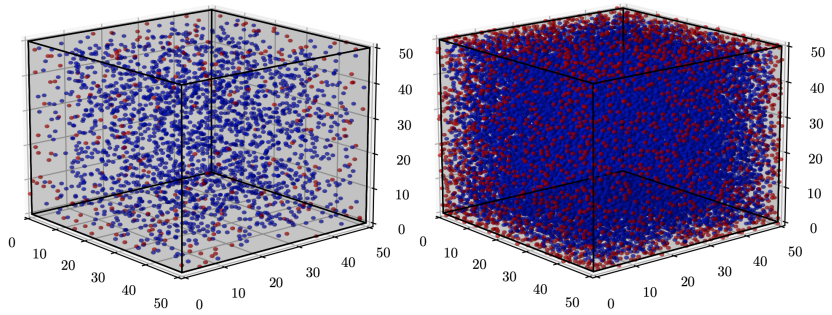

(a) $p = 1\%$, $r_b = 0.5$: $f_V^{pul} = 0.066$

(b) $p = 10\%$, $r_b = 0.5$: $f_V^{pul} = 0.128$

(c) $p = 1\%$, $r_b = 1$: $f_V^{pul} = 0.061$

(d) $p = 10\%$, $r_b = 1$: $f_V^{pul} = 0.122$

Figure 3.7. Example of generated pore structures at different porosity levels p and bubble radii r_b, with the fragment size fixed at $l_f = 50$ μm [49, 67]. Pores completely contained in the fragment are shown in blue, whereas pores opened during pulverization (i.e., in contact with the fragment surface) are shown in red. For each pore structure, f_V^{pul} is provided. Note that due to the random nature of the algorithm, different f_V^{pul} can be obtained for the given porosity and bubble radius values.

Different pore structures with relevant characteristics are therefore generated using the Python script. For each porosity and bubble radius-to-fragment-size ratio, 100 pore structures are generated so that the potential statistical variations in f_V^{pul} can be shown. The results are provided in Fig. 3.8. The data generated by the Python script are fitted using a linear regression, resulting in

$$f_V^{pul} = c_p p + c_r \frac{r_b}{l_f} + c_0, \tag{3.22}$$

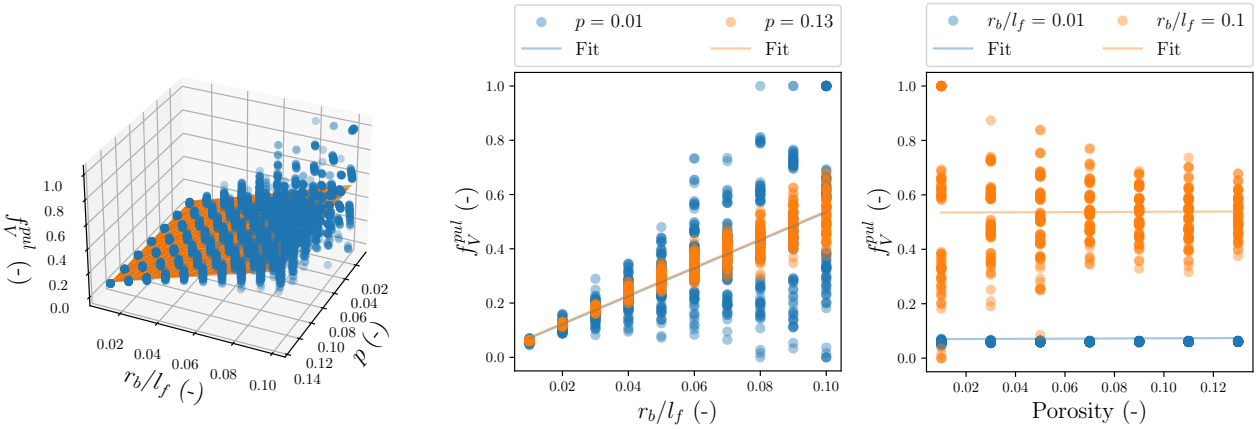

(a) (b) (c)

Figure 3.8. Predicted f_V^{pul} values for different pore structures in fuel fragments, along with a fit using a linear regression. (a) shows the data in 3-D. (b, c) show the data along r_b/l_f for extreme porosity values and along the porosity for extreme r_b/l_f values, respectively. f_V^{pul} does not significantly depend on porosity but increases on average with r_b/l_f. Despite an appropriate fitting, the quality of the fit is equal to $R^2 = 0.79$, due to large variations in f_V^{pul} for some pore structures, especially for low porosities.

with $c_p = 0.03$ (-) the coefficient for the porosity, $c_r = 5.17$ (-) the coefficient for the bubble-radius-to-fragment-size ratio, and $c_0 = 0.02$ (-) the constant. f_V^{pul} does not vary significantly with porosity but increases on average with r_b/l_f. Note that c_0 is, as expected, close to 0. The amount of tFGR due to pulverization should indeed tend toward 0 when the porosity decreases. It is important to note that although the fit follows the average trend of f_V^{pul} quite successfully, the quality of the fit is as low as $R^2 = 0.79$. This is due to the fact that, for some pore structures, the random nature of the pore placement leads to large variations in f_V^{pul} values. This is especially true for lower porosities and large r_b/l_f values (see Figs. 3.8b and 3.8c) since the position of a few large bubbles significantly affects f_V^{pul}.

3.5 Summary

Once we refactored Sifgrs's implementation in BISON and made it significantly more modular and extensible (see Chapter 2), we were able to implement a new tFGR model. The model extends the existing low-burnup Sifgrs capabilities to HBu conditions. It relies on semi-empirical and mechanistic models to describe HBS formation, transfer of fission gases from the NR to the HBS region, HBS intragranular fission gas generation and diffusion, HBS bubble evolution, fuel pulverization, and the resulting sudden release of fission gases.

The model has been successfully tested, verified, and implemented in the fuel performance code BISON. The model tracks bubble populations and bubble pressures in the fuel both in the NR and HBS regions and provides an estimate of the tFGR from fuel pulverization that is sensitive to the fuel microstructure and operating conditions, as requested for the milestone.

Now that this capability has been developed within the refactored Sifgrs, future expansion is possible. Future work will focus on improving the description of this model by validating the separate aspects of it, identifying gaps and inaccuracies, and proposing improvements. Moreover, since the current tFGR model only happens during fuel pulverization, more release mechanisms will be investigated. Furthermore, one of the limitations of the current model is that it only accounts for HBS formation at the pellet rim where the burnup is high and temperatures are low. However, other microstructural changes have been observed, including the formation of a dark zone deeper within the pellet [20]. Future work should also include this other microstructral change.

4. COMPARISON OF THE EMPIRICAL AND MECHANISTIC tFGR MODELS

4.1 Discussions on the Differences between the Empirical and Mechanistic Approaches

The empirical model takes in the temperature and the local burnup and defines the percentage of FGR [21]. It performs well in conditions (temperature, heating rate, irradiation history, burnup, fuel properties, etc.) close to the ones in which the fitted experimental data was obtained. As such, it is a valuable improvement compared to previous Sifgrs capabilities in HBu transient scenarios. However, it has limitations. Although it provides a general idea of how temperature and local burnup potentially affect FGR, it does not provide a mechanistic understanding of the release phenomena. As a result, the quality of its predictions degrades when applied to other conditions, as shown in Fig. 3.2 [21]. As described in Ref. [21], there is a crucial need for a mechanistic model that physically describes the physical phenomena of FGR in HBS transient conditions. Such a model could be used to better predict fuel behavior and would be applicable to a wide range of operating conditions.

The model described in Chapter 3 is an attempt to develop such a mechanistic model. Although in a preliminary stage, it describes many phenomena leading to tFGR that are not accounted for in the empirical model. The differences between the empirical and the mechanistic models are listed in Table 4.1. The new mechanistic model accounts for HBS formation [16], details fission gas behavior during the transition from non-restructured to HBS fuel, describes HBS pore evolution [61], and provides criteria for fuel pulverization and the subsequent release of fission gases [18]. These mechanistic stages are informed by experimental data analysis [16, 61] and lower length scale modeling efforts [18, 61]. Since it does not model all of the intermediate steps, the empirical model is computationally slightly cheaper than the mechanistic model, although both provide appropriate performances for fuel performance modeling.

4.2 Comparison of Model Performance on Assessment Cases

To compare the performance of the empirical and mechanistic models, we ran both models on the Studsvik 191 rod, which was part of an integral LOCA research program and reached HBu [70, 71]. This case is a readily available assessment case available in BISON [72], and most of the description provided below is taken directly from the BISON

Table 4.1. Comparison of the different features between the empirical and mechanistic model.

Feature	Mechanistic model (see Chapter 3)	Empirical model [21]
Models HBS formation	✓	
Models fission gas transfer from NR to HBS fuel	✓	
Models HBS pore evolution	✓	
Determines swelling from HBS fuel	✓	
Models fuel pulverization	✓	
Can inform axial relocation	✓	
Models tFGR release	✓	✓
Integrated with Sifgrs	✓	✓
Can be combined with microcracking model [13]	✓	
Computationally cheaper		✓
Can be improved with experimental data	✓	✓
Can be improved with mechanistic lower length scale modeling	✓	

documentation. The input files were updated to use the empirical and mechanistic models.

4.2.1 Description of the assessment case

The Studsvik LOCA tests were completed as part of an integral LOCA research program sponsored by the NRC to investigate the mechanical properties of ballooned and ruptured cladding as well as the behavior of highly irradiated fuel during the transient [70].

The test series consisted of six integral tests. The majority of these experiments observed severe fuel fragmentation and dispersal. Only two rods have been analyzed with BISON this far, Rods 191 and 196. These were chosen to demonstrate that the existing pulverization models within BISON are able to predict whether or not fine fragmentation will occur the possibility of fuel dispersal. In this report, we use Rod 191 as it went to a higher burnup (70 MWd/kgU vs. 55 MWd/kgU for rod 196).

The fabrication characteristics of the analyzed Studsvik rods are from [70, 71]. The test rods were segmented commercially irradiated rods. The fuel and cladding materials are UO_2 and ZIRLO. The refabricated rods were backfilled with helium. The rods were base irradiated to desired burnups (i.e., around 70 MWd/kgU for rod 191). After the base irradiation the rodlets were refabricated and inserted into the Studsvik test train inside a hot cell. The experimental specimens are subjected to external heating at a rate of 5°C/s to the target peak cladding temperature. This temperature was 1160°C for Rod 191. More information is available in the BISON documentation.

4.2.2 Results

Figure 4.1 shows the FGR predictions from Sifgrs with the empirical and the mechanistic tFGR model. The empirical tFGR model (labeled as FGR + empirical tFGR in Fig. 4.1) predicts a small amount of FGR at the end of base irradiation (around 1.2% vs. around 1.0% with only FGR). However, it predicts significant tFGR during the heat up phase of the LOCA, reaching a total release fraction of almost 9%.

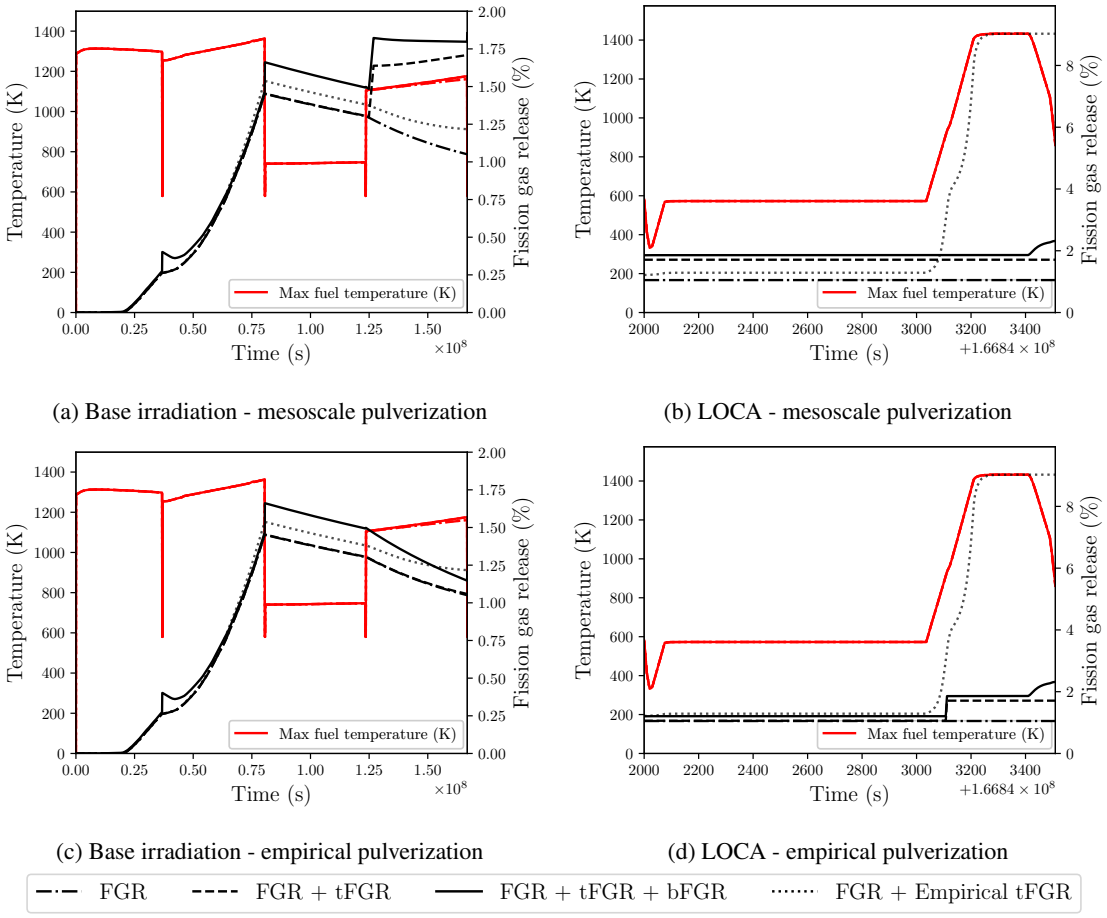

(a) Base irradiation - mesoscale pulverization

(b) LOCA - mesoscale pulverization

(c) Base irradiation - empirical pulverization

(d) LOCA - empirical pulverization

Figure 4.1. Comparison of the FGR predictions from the purely diffusional model (FGR), the mechanistic tFGR model (FGR + tFGR), the mechanistic tFGR model with the microcracking burst FGR model (FGR + tFGR + bFGR), and the empirical (FGR + Empirical tFGR). The results for base irradiation (a, c) and the LOCA scenario (b, d) are shown. (a, b) show the results using the mechanistic pulverization model from Section 3.3.2, and (c, d) show the results for the empirical pulverization model from Section 3.3.1.

To better understand the different FGR contributions in the case of the mechanistic FGR, Fig. 4.1 shows the different contributions to release. It shows the amount released from diffusional FGR alone (FGR), from the mechanistic tFGR model (FGR + tFGR), and from the mechanistic tFGR model with the microcracking burst FGR model [13] (FGR + tFGR + bFGR). This highlights at what point does burst FGR or tFGR happen. For example, burst FGR is predicted to happen during large temperature variations during base irradiation. Sharp jumps in FGR are observed during the transition from the first cycle to the second and from the second to the third. Moreover, some burst FGR happens during cool down in the latest part of the LOCA transient.

The contribution from mechanistic tFGR depends on the pulverization model used, and two different sets of results

of the mechanistic tFGR are presented in Fig. 4.1 dependent on which pulverization model is used. One set of results uses the empirical criteria for pulverization (see Section 3.3.1) and is shown in Figs. 4.1c and 4.1d. The other uses the mesoscale-informed criteria (see Section 3.3.2 and Ref. [18]) and is shown in Figs. 4.1a and 4.1b. Since the mechanistic tFGR model captures the release due to pulverization, both models predict different release behavior. Although both predict the same final amount of FGR in this case, with the outer rim of the fuel fully pulverized, tFGR happens at two different times. When using the mesoscale-informed criteria for pulverization, fuel pulverization and tFGR are predicted to happen as the third cycle of base irradiation begins. Note that no tFGR happens during the heating phase of the LOCA transient in that case because all the HBS structure has already pulverized, and no other release mechanism is accounted for. This result is not physical and will be discussed further below (see Fig. 4.2). When using the empirical pulverization criteria, it happens during the heat up phase of the LOCA transient. In both cases, the final FGR is around 2%, even when accounting for burst FGR, which is around half of what is predicted with the empirical model.

The conclusions drawn from the pulverization model predictions need to be nuanced, though, as the model is still being developed, tested, and validated. When using the mechanistic pulverization criteria, pulverization is being predicted prematurely due to the inadequate description of HBS bubble radius evolution. Currently, the HBS bubble radius is initially set to 0 m, and only starts to evolve once the HBS volume fraction reaches a threshold value (set to 0.5) [18]. However, the same threshold is used for fuel pulverization Section 3.3.2. As a result, when the HBS volume fraction reaches the threshold value, HBS bubble radius is close to 0, and internal pressure is artificially high, leading to fuel pulverization. This phenomenon is illustrated in Fig. 4.2. To ensure realistic model prediction, HBS bubble radius evolution needs to be start earlier in the HBS formation process so that HBS bubble reach a reasonable size as the HBS volume fraction threshold for pulverization is reached. Moreover, the effect of mesh size on the predicted pulverized volume is being investigated in a concurrent NEAMS milestone. Future work should incorporate this insight to provide

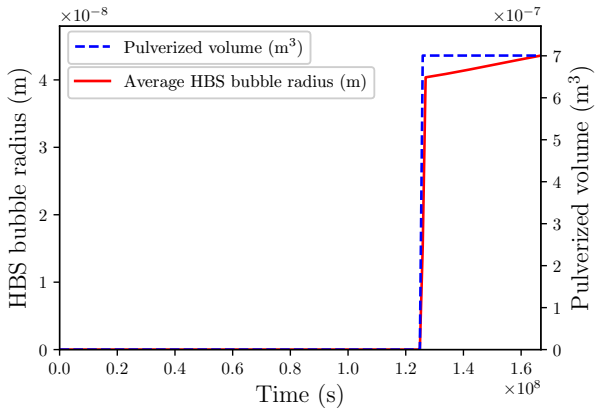

Figure 4.2. HBS bubble radius and pulverization volume evolution during base irradiation of the Studsvik case (Rod 191). Pulverization is prematurely predicted due to the high pressure in unphysically small HBS bubbles. The HBS bubble size is underestimated because it only starts evolving once the HBS volume fraction threshold (0.5) is reached. This bubble evolution model will be fixed in future work.

reliable tFGR predictions.

Unfortunately, the amount of FGR was not experimentally measured for this Studsvik case, so validation is not possible. This exercise, however, shows the influence of the pulverization criteria on the predicted tFGR and suggests that the mechanistic approach might underestimate FGR during the heat up phase of the LOCA. Additional mechanisms might be at play.

4.2.3 Conclusion and future work

We discussed the different features of the empirical tFGR developed in Ref. [21], and the mechanistic model developed in this report. Then, using Rod 191 of the Studsvik HBu LOCA tests, we quantified the different predictions of the two approaches, including, for the mechanistic model, two different criteria. This effort highlighted the importance of the pulverization criteria used in the mechanistic tFGR model, as the choice of criteria influences when pulverization and the resulting tFGR occurs. It also highlighted the need to improve the HBS bubble growth model. When using the mesoscale-informed criterion for fuel pulverization, the mechanistic model seems to underestimate FGR during LOCA since pulverization happened earlier. However, more extensive model development and validation data are needed to draw definitive conclusions.

Microstructure data and experimental measurements of FGR in HBu conditions during normal operations and transients are needed. As more validation cases become available, different aspects of the model can be validated and improved. In particular, HBu cases with FGR and FGR that also provide fuel microstructure characterization would be extremely valuable. In the meantime, the mechanistic model will be further developed and improved by following the roadmap presented in Ref. [21] and reproduced in Fig. 3.3.

5. BENCHMARKING OF BISON FISSION GAS RELEASE CAPABILITIES

5.1 Description of the NEA Benchmarking Activity

FGR has a significant impact on nuclear fuel performance. Fuel performance codes therefore model fission gas behavior but with varying degrees of detail and accuracy. In general, diffusion-based FGR models are well established and validated for steady state conditions. Under transient conditions, however, FGR is known to be dominated by burst mechanism not captured by diffusion-based models. Appropriate models for these conditions are not as universally implemented in fuel performance codes, and their accuracy has not yet been thoroughly established.

The OECD NEA Expert Group on Reactor Fuel Performance is leading a benchmark to compare fuel performance code predictions against experimental data and against themselves. The benchmark aims to challenge the models during transients representative of anticipated operational occurrences. Selected experimental cases have transient powers high enough to ensure burst FGR but low and short enough to ensure that diffusional FGR was minimal. The goals of the benchmarking activity are to enhance the understanding of burst FGR mechanisms and facilitate the improvement of fuel performance code models for transient conditions (or develop new ones), therefore reducing uncertainties and increasing margin to fuel performance limits.

For benchmark participants to use real, integral rod irradiation data, two experimental cases have been selected for the benchmark. In both cases, the rod undergoes base irradiation before being re-irradiated in transient conditions. The conditions are such that burst FGR takes place, but diffusional FGR is expected to be minimal during the transient. Moreover, irradiation history, rod characteristics, and PIE data was needed for validation. With these criteria in mind, the REGATE and HATAC-C2 cases were selected.

Participants are expected to model the irradiation histories of the REGATE and HATAC cases with three different model configurations:

1. The first one should not have any model for burst FGR. This configuration reveals how much diffusional FGR is predicted by the fuel performance codes. It is expected to underestimate FGR in transient conditions.
2. The second one should involve a burst FGR model and hopefully provide accurate predictions of experimentally measured total FGR.
3. The third one should also involve a burst FGR model but add an additional 5% to the rod power. This case provides information on the sensitivity of the model with respect to power. It is expected to lead to an increase

in burnup, temperature, and FGR.

5.2 Description of the Two Cases of Interest

The REGATE and HATAC-C2 specifications are available from the IFPE database. Please request from the NEA Databank via the standard route for IFPE requests. The subsections below quickly describe the two cases.

5.2.1 REGATE

The REGATE case is a French Alternative Energies and Atomic Energy Commission (CEA) experiment which aimed to study FGR and fuel swelling during a power transient at medium burnup. The base rod was irradiated in Gravelines-5 PWR to 47 MWd/kgU. The rod segment selected for the REGATE case was then re-irradiated in the Siloé test reactor without refabrication. Non-destructive PIE was performed after base irradiation (including FGR measurements), and both destructive and non-destructive PIE were performed after re-irradiation (including FGR).

5.2.2 HATAC-C2

The HATAC-C2 case aimed to investigate stable and radioactive fission gas release behavior under power cycling. The sample is a segment cut from a commercially irradiated parent rod. The parent rod was irradiated in Fessenheim-2 PWR to 46 MWd/kgU, and the segment rod was re-irradiated in the Siloé test reactor. The segment rod was fitted with gas flow lines for continuous refabrication. Gas release measurements were obtained after each transient by spectrometry, and PIE was obtained for both parent rod and segment segment.

5.3 Modeling Choices

BISON offers many different models, options, and parameter values for each aspect of fuel performance. Although we will not do any fine tuning of model parameters for this exercise, modeling the REGATE and HATAC case requires selecting the most appropriate models for the conditions of interest. Below, we provide a high-level description of the modeling choices made for the NEA activity. The same models are used for both cases.

For thermal conductivity and specific heat capacity, the well established NFIR model is used to diffuse the heat generated in the fuel [73, 74]. Moreover, a correction based on Ref. [75] is applied in HBS to accounted for the higher porosity. The gap conductivity accounts for the gas composition, and the Lanning model is used to determine the jump distance [76]. In the cladding, the MATPRO model is used [77].

Within Sifgrs, the default values listed in Tables 2.1 to 2.3 were used, except for a few options to use the latest, most accurate models. Rather than the Formas algorithm [5], we used Polypole2 to be able to model the non-equilibrium trapping and detrapping of fission gases to and from intragranular bubbles [8]. Using Polypole2 is especially relevant in transient conditions where the quasi-steady-state assumption made by the Formas and Polypole1 algorithms does not apply. When modeling burst FGR, we add the model from Ref. [13] to account for microcracking during temperature transient and the resulting release. In addition, we use the HBS model described in Chapter 3 using Barani's

JMAK model for HBS formation. Potential pulverization and tFGR are also accounted for when burst FGR models are activated.

Microstructure evolution is in large part governed by Sifgrs since it provides intragranular and intergranular bubble population. However, grain size is calculated by a different model. Here, we use the model published in Ref. [78], which mechanistically describes UO_2 grain growth under irradiation. In the cladding, zirconium oxidation is also accounted for.

To describe the mechanical behavior of the fuel and cladding, we leverage BISON capabilities to model volumetric changes due to thermal expansion and volumetric swelling in the fuel and thermal expansion and irradiation growth in the cladding. Both the fuel and cladding behavior include creep. Note that the pull of gravity is also accounted for.

5.4 Preliminary BISON Results

5.4.1 REGATE

Preliminary results for the REGATE case are presented in Figs. 5.1 and 5.2. Fig. 5.1 shows the burnup predictions, and Fig. 5.2 shows the temperature and FGR predictions during base irradiation and re-irradiation. Fig. 5.2 shows the results in three different scenarios dictated by the NEA benchmarking guidelines: BISON predictions are computed (1) without any model for burst release of fission gases, (2) with the burst release model activated [13], and (3) with the burst model, and a 5% increase in power. Although BISON's predictions are compared to experimental data and other codes' predictions as part of the benchmark activity, we only show the experimental data in this report, which BISON matches quite well.

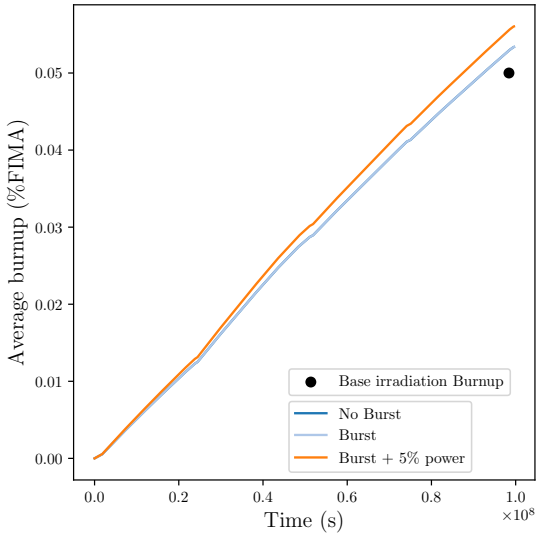

Figure 5.1. Burnup prediction from BISON for the REGATE case, compared against the reported value.

The burnup shown in Fig. 5.1 slightly overpredicts the base irradiation burnup but not significantly. The difference is minimal and validates the BISON prediction. With the additional 5% in power, the final burnup increases, as expected.

BISON's FGR predictions closely match the experimental data, both at the end of base irradiation and at the end of re-irradiation in the Siloé reactor. Without the burst model activated, the predictions at the end of base irradiation fall almost exactly on top of the experimental measurement (see Fig. 5.2a). However, without a mechanism for burst release, the amount of FGR predicted at the end of the transient is slightly more than half of the measured amount (see Fig. 5.2b). When using the burst release model from Ref. [13], the amount of predicted FGR increases slightly during base irradiation and increases significantly during re-irradiation, getting close to PIE data (see Figs. 5.2c and 5.2d). The amount of FGR at the end of the transient is slightly underestimated, but BISON's accuracy in predicting both base irradiation and re-irradiation FGR is remarkable, especially without any tuning of the parameters for this particular case.

As expected, the increase in power leads to an increase in FGR both during base irradiation and re-irradiation. With the additional 5% in power, the FGR predictions are higher than the experimental data, as shown in Figs. 5.2e and 5.2f.

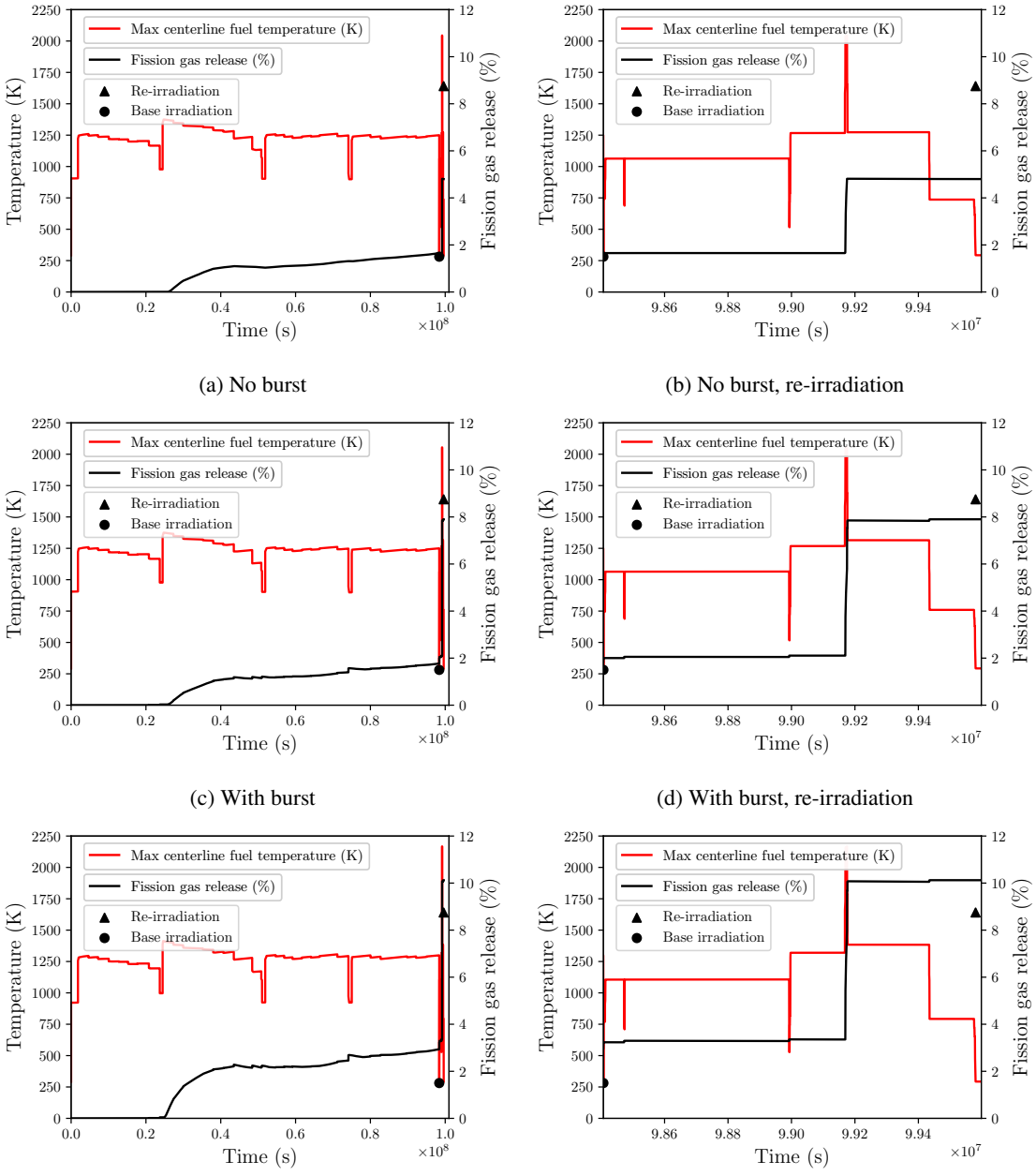

(a) No burst

(b) No burst, re-irradiation

(c) With burst

(d) With burst, re-irradiation

(e) With burst and +5% power

(f) With burst and +5% power, re-irradiation

Figure 5.2. Temperature history and FGR predictions from BISON for the REGATE case. The figures show the results (a, b) without burst model being used, (c, d) with the burst model from [13], which matches PIE data, and (e, f) with the same burst model and an +5% increase in power. (a, c, e) show the results from the whole irradiation history; (b, d, f) focus on the re-irradiation history.

5.4.2 HATAC-C2

As in Section 5.4.1 for REGATE, the preliminary results for the HATAC case are presented in Figs. 5.3 and 5.4. Fig. 5.3 shows the burnup predictions, and Fig. 5.4 shows the temperature and FGR predictions during base irradiation and re-irradiation. The burnup shown in Fig. 5.3 slightly overpredicts the base irradiation burnup but not significantly. The difference is minimal and validates the BISON prediction. With the additional 5% in power, the final burnup increases, as expected.

BISON's FGR predictions for the HATAC closely match the experimental data at the end of base irradiation. Without the burst model activated, the predictions at the end of base irradiation fall almost exactly on top of the experimental measurement (see Fig. 5.4a). However, without a mechanism for burst release, the amount of FGR predicted at the end of the transient is significantly less than the measured amount (see Fig. 5.4b). When using the burst release model from Ref. [13], the amount of predicted FGR increases slightly during base irradiation and increases significantly during re-irradiation, getting closer to PIE data (see Figs. 5.4c and 5.4d). The amount of FGR at the end of the transient remains underestimated, but BISON's accuracy in predicting both base irradiation and re-irradiation FGR is satisfactory, especially without any tuning of the parameters for this particular case. Current mechanisms seem to underestimate transient release, or additional release mechanisms could be at play at HBu during transients.

As expected, the increase in power leads to an increase in FGR both during base irradiation and re-irradiation. With the additional 5% in power, the FGR predictions are higher than the experimental data, as shown in Figs. 5.4e and 5.4f. Note, however, that in the current version of the figure, the results in Figs. 5.4e and 5.4f do not reach the end of re-irradiation due to convergence issues.

Some HBS formation, fuel pulverization, and tFGR release are predicted for the HATAC case. The tFGR model

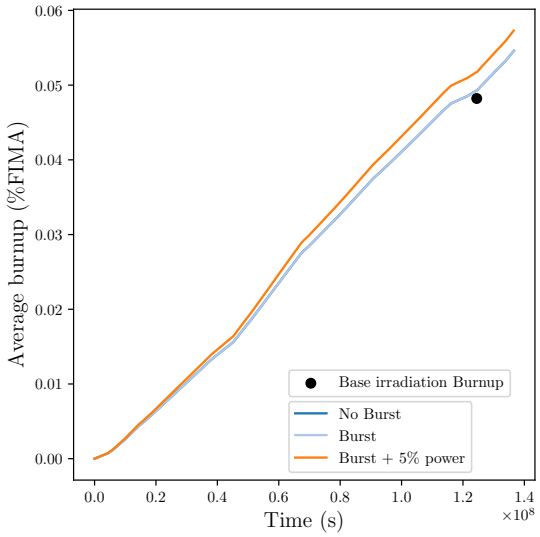

Figure 5.3. Burnup prediction from BISON for the HATAC case, compared against the reported value. Note that the "Burst" case with +5% power has not converged until the end of re-irradiation.

developed and implemented in this report predicts release in addition to the burst release due to microcracking described in Ref. [13].

5.5 Summary and Future Work

BISON—with the updated version of `Sifgrs` implemented in this report—was used to participate in an NEA benchmarking activity. The goal of the effort is to compare different fuel performance codes' ability to model FGR during base irradiation and during transient scenarios. Since the activity is ongoing, this report describes preliminary BISON results and comparisons against experimental data. The results show that BISON adequately predicts FGR in conditions relevant to both the REGATE and HATAC cases. The results also highlight the importance of a burst FGR model that describes fuel microcracking during transients. Without it, the amount of FGR was significantly underpredicted. The HATAC case also showed the importance of the newly developed and implemented tFGR model described in Chapter 3.

Future work includes completing of the NEA activity and identifying potential gaps in BISON's capabilities and performance by comparing it to other codes. To complete the NEA activity, one important step will be to select the same parameters and geometry for all participants to ensure code-to-code comparison rather than seeing the impact of user assumptions. Some parameters are not clearly defined in the REGATE and HATAC reports, which lead different users to make different assumptions. For example, the refabricated gas internal pressure for HATAC was not specified, leading users to pick values ranging from 0.1 to 0.4 MPa. Ensuring that all participants use the same values and conditions will improve the quality of the benchmark. Once done, we will rerun the simulation shown in this section with the finalized parameters and compare code predictions.

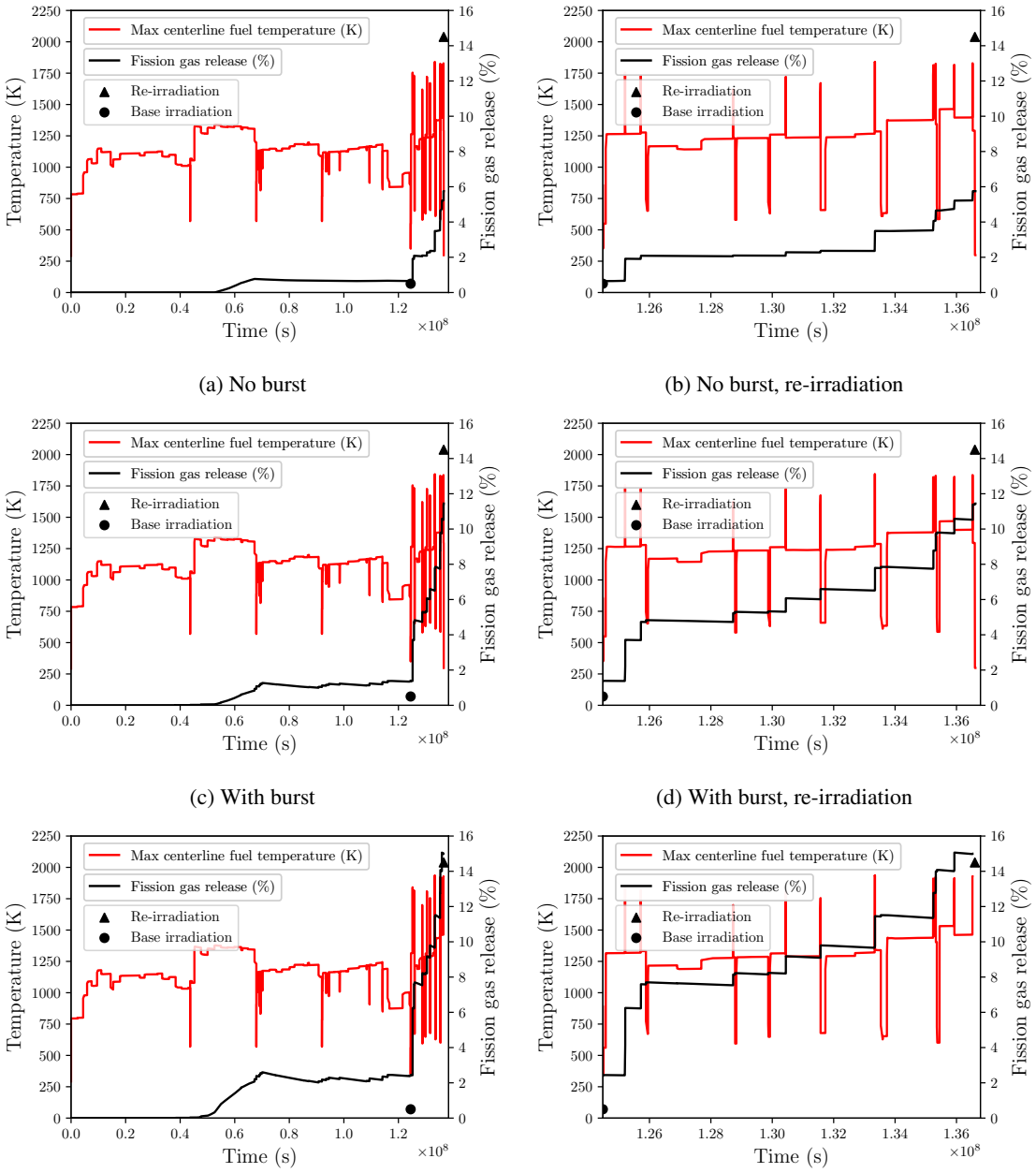

(a) No burst

(b) No burst, re-irradiation

(c) With burst

(d) With burst, re-irradiation

(e) With burst and +5% power

(f) With burst and +5% power, re-irradiation

Figure 5.4. Temperature history and FGR predictions from BISON for the HATAC case. The figures show the results (a, b) without burst model being used, (c, d) with the burst model from [13], which matches PIE data, and (e, f) with the same burst model and an +5% increase in power. (a, c, e) show the results from the whole irradiation history; (b, d, f) focuses on the re-irradiation history. Note that the "Burst" case with +5% power has not converged until the very end of re-irradiation.

6. OVERALL CONCLUSIONS AND FUTURE WORK

This report details the work performed for the Level 2 NEAMS milestone titled "Compare predictions of transient fission gas release by empirical and mechanistic models to experiments in HBu UO_2 fuel." More than just a comparison between two existing models, the work described here consisted of (1) refactoring the implementation of the Sifgrs model in BISON to support new capabilities, (2) developing a new mechanistic model for tFGR resulting from HBS pulverization in Sifgrs, (3) comparing the empirical tFGR model developed in parallel to the mechanistic model using one of the Studsvik HBu LOCA assessment cases, and (4) benchmarking BISON against other fuel performance codes for burst and transient FGR through an NEA activity. The main achievements and conclusions are listed below:

- Sifgrs was refactored to expend its capabilities to new fuel forms (e.g., UN) and new conditions (e.g., HBu conditions). As such, we increased the amount and quality of tests, we made major changes to the code structure to make it more modular and decrease code duplication, and we increased documentation and made the code more user friendly. The updated implementation of Sifgrs enabled the quick and efficient development of fission gas release and swelling capabilities for UN fuel [26], and the addition of HBS capabilities, which was one of the main areas of focus of the current milestone, is described in Chapter 3.

- A new mechanistic HBu tFGR model was developed and implemented in Sifgrs. The model extends the existing low-burnup Sifgrs capabilities to HBu conditions. It relies on semi-empirical and mechanistic models to describe HBS formation, transfer of fission gases from the NR to the HBS region, HBS intragranular fission gas generation and diffusion, HBS bubble evolution, fuel pulverization, and the resulting sudden release of fission gases. As such, the model combines different models in a consistent, coupled way within Sifgrs. The model has been tested, verified, and merged into BISON. The model mechanistically describes tFGR due to the pulverization of the HBS and is sensitive to the fuel microstructure and operating conditions. The current implementation focused on the rim HBS. However, it was developed such that it can be extended to the dark zone deeper within the pellet [20].

- The new mechanistic model was then compared with a new empirical tFGR model published in Ref. [21]. We discussed the different features of the models and then used them to predict FGR in rod 191 from the Studsvik HBu LOCA tests. This test does not have direct FGR measurements to validate the models with, but we compared the behavior of the two models. In particular, we tested two versions of the mechanistic tFGR model: one using an empirical criteria for fuel pulverization and another one leveraging some recent developments from lower length scale modeling efforts [17, 18]. The model predictions are discussed, and current gaps are identified.

- BISON—with the updated version of Sifgrs implemented in this report—was used to participate in an NEA benchmarking activity. The goal of the effort is to compare different fuel performance codes' abilities to model FGR during base irradiation and transient scenarios. Since the activity is ongoing, this report describes preliminary BISON results and comparison against experimental data. The results show that BISON adequately predicts FGR in conditions relevant to both the REGATE and HATAC cases.

Future work should focus on improving and expanding the current Sifgrs capabilities. In particular, developing new models for fission gas transport and release from HBS should be a priority to support the needs of the nuclear industry. Validating and benchmarking these models are also crucial to ensure that these models accurately describe the mechanisms of fuel microstructure evolution and fission gas release. Moreover, extending the newly developed HBS capabilities to the dark zone region observed deeper inside the fuel pellet [20] would improve BISON's predictive capabilities and help extend fuel utilization to higher burnups.

Bibliography

[1] U.S. Nuclear Regulatory Commission (NRC). *RIL 2021-13, Interpretation of Research on Fuel Fragmentation, Relocation, and Dispersal at High Burnup*. (ADAMS Proprietary Accession No. ML21313A110), 2021.

[2] F. Cappia et al. "Critical assessment of the pore size distribution in the rim region of high burnup UO2 fuels". In: *Journal of Nuclear Materials* 480 (Nov. 2016), pp. 138–149. ISSN: 0022-3115. DOI: 10.1016/J.JNUCMAT.2016.08.010.

[3] Nathan Capps et al. "A Critical Review of High Burnup Fuel Fragmentation, Relocation, and Dispersal under Loss-Of-Coolant Accident Conditions". In: *Journal of Nuclear Materials* 546 (Apr. 2021), p. 152750. ISSN: 0022-3115. DOI: 10.1016/J.JNUCMAT.2020.152750.

[4] Giovanni Pastore et al. "Physics-based modelling of fission gas swelling and release in UO2 applied to integral fuel rod analysis". In: *Nuclear Engineering and Design* 256 (Mar. 2013), pp. 75–86. ISSN: 0029-5493. DOI: 10.1016/J.NUCENGDES.2012.12.002.

[5] P. Hermansson and A. R. Massih. "An effective method for calculation of diffusive flow in spherical grains". In: *Journal of Nuclear Materials* 304 (2-3 Aug. 2002), pp. 204–211. ISSN: 0022-3115. DOI: 10.1016/S0022-3115(02)00873-5.

[6] K. Lassmann and H. Benk. "Numerical algorithms for intragranular fission gas release". In: *Journal of Nuclear Materials* 280 (2 July 2000), pp. 127–135. ISSN: 0022-3115. DOI: 10.1016/S0022-3115(00)00044-1.

[7] Giovanni Pastore et al. "Uncertainty and sensitivity analysis of fission gas behavior in engineering-scale fuel modeling". In: *Journal of Nuclear Materials* 456 (Jan. 2015), pp. 398–408. ISSN: 0022-3115. DOI: 10.1016/J.JNUCMAT.2014.09.077.

[8] G. Pastore et al. "An effective numerical algorithm for intra-granular fission gas release during non-equilibrium trapping and resolution". In: *Journal of Nuclear Materials* 509 (Oct. 2018), pp. 687–699. ISSN: 0022-3115. DOI: 10.1016/J.JNUCMAT.2018.07.030.

[9] T. Barani et al. "Modeling intra-granular fission gas bubble evolution and coarsening in uranium dioxide during in-pile transients". In: *Journal of Nuclear Materials* 538 (Sept. 2020), p. 152195. ISSN: 0022-3115. DOI: 10.1016/J.JNUCMAT.2020.152195.

[10] T. Barani et al. "Multiscale modeling of fission gas behavior in U3Si2 under LWR conditions". In: *Journal of Nuclear Materials* 522 (Aug. 2019), pp. 97–110. ISSN: 0022-3115. DOI: 10.1016/J.JNUCMAT.2019.04.037.

[11] D. Pizzocri et al. “PolyPole-1: An accurate numerical algorithm for intra-granular fission gas release”. In: *Journal of Nuclear Materials* 478 (Sept. 2016), pp. 333–342. ISSN: 0022-3115. DOI: 10.1016/J.JNUCMAT.2016.06.028.

[12] D. Pizzocri et al. “A model describing intra-granular fission gas behaviour in oxide fuel for advanced engineering tools”. In: *Journal of Nuclear Materials* 502 (Apr. 2018), pp. 323–330. ISSN: 0022-3115. DOI: 10.1016/J.JNUCMAT.2018.02.024.

[13] T. Barani et al. “Analysis of transient fission gas behaviour in oxide fuel using BISON and TRANSURANUS”. In: *Journal of Nuclear Materials* 486 (Apr. 2017), pp. 96–110. ISSN: 0022-3115. DOI: 10.1016/J.JNUCMAT.2016.10.051.

[14] D. A. Andersson et al. “Atomistic modeling of intrinsic and radiation-enhanced fission gas (Xe) diffusion in UO2±x: Implications for nuclear fuel performance modeling”. In: *Journal of Nuclear Materials* 451 (1-3 Aug. 2014), pp. 225–242. ISSN: 0022-3115. DOI: 10.1016/J.JNUCMAT.2014.03.041.

[15] Anders David Andersson. *Density functional theory calculations of defect and fission gas properties in U-Si fuels*. Los Alamos National Laboratory (LANL), LA-UR-15-27996, Feb. 2016. DOI: 10.2172/1237246. URL: http://www.osti.gov/servlets/purl/1237246/.

[16] T. Barani et al. “Modeling high burnup structure in oxide fuels for application to fuel performance codes. part I: High burnup structure formation”. In: *Journal of Nuclear Materials* 539 (Oct. 2020), p. 152296. ISSN: 0022-3115. DOI: 10.1016/J.JNUCMAT.2020.152296.

[17] L. K. Aagesen et al. *Mesoscale simulations to inform microstructure- based pulverization criterion in high-burnup UO_2*. Tech. rep. INL/EXT-21-64275. Idaho National Laboratory, 2021.

[18] Larry Kenneth Aagesen Jr et al. “Implementation and testing of physics-based pulverization model in Bison”. In: (Sept. 2022). DOI: 10.2172/1984930. URL: https://www.osti.gov/servlets/purl/1984930/.

[19] J. A. Turnbull et al. “An Assessment of the Fuel Pulverization Threshold During LOCA-Type Temperature Transients”. In: *Nuclear Science and Engineering* 179 (2015), pp. 477–485.

[20] Casey McKinney et al. “Characterization of the radial microstructural evolution in LWR UO2 using electron backscatter diffraction”. In: *Journal of Nuclear Materials* 585 (Nov. 2023), p. 154605. ISSN: 0022-3115. DOI: 10.1016/J.JNUCMAT.2023.154605. URL: https://linkinghub.elsevier.com/retrieve/pii/S0022311523003720.

[21] Nathan Capps et al. “Empirical and mechanistic transient fission gas release model for high-burnup LOCA conditions”. In: *Journal of Nuclear Materials* 584 (Oct. 2023), p. 154557. ISSN: 0022-3115. DOI: 10.1016/J.JNUCMAT.2023.154557.

[22] R. O.A. Hall, M. J. Mortimer, and D. A. Mortimer. “Surface energy measurements on UO2 — A critical review”. In: *Journal of Nuclear Materials* 148 (3 May 1987), pp. 237–256. ISSN: 0022-3115. DOI: 10.1016/0022-3115(87)90017-1.

[23] Toshiaki Kogai. “Modelling of fission gas release and gaseous swelling of light water reactor fuels”. In: *Journal of Nuclear Materials* 244 (2 Apr. 1997), pp. 131–140. ISSN: 0022-3115. DOI: 10.1016/S0022-3115(96)00731-3.

[24] Yinbin Miao et al. “Gaseous swelling of U3Si2 during steady-state LWR operation: A rate theory investigation”. In: *Nuclear Engineering and Design* 322 (Oct. 2017), pp. 336–344. ISSN: 0029-5493. DOI: 10.1016/J.NUCENGDES.2017.07.008.

[25] Benjamin Beeler et al. “Molecular dynamics investigation of grain boundaries and surfaces in U3Si2”. In: *Journal of Nuclear Materials* 514 (Feb. 2019), pp. 290–298. ISSN: 0022-3115. DOI: 10.1016/J.JNUCMAT.2018.12.008.

[26] Jason Rizk et al. *Development of Mechanistic Fission Gas Release and Swelling Models for UN Fuels in BISON*. Tech. rep. Los Alamos National Laboratory, July 2023.

[27] G Pastore et al. “Modeling Fission Gas Behaviour with the BISON Fuel Performance Code”. In: (2017). URL: http://www.inl.gov.

[28] K. Lassmann et al. “Modelling the high burnup UO2 structure in LWR fuel”. In: *Journal of Nuclear Materials* 226 (1-2 Oct. 1995), pp. 1–8. ISSN: 0022-3115. DOI: 10.1016/0022-3115(95)00116-6.

[29] Larry K. Aagesen et al. “Phase-field simulations of fission gas bubbles in high burnup UO2 during steady-state and LOCA transient conditions”. In: *Journal of Nuclear Materials* 557 (Dec. 2021), p. 153267. ISSN: 0022-3115. DOI: 10.1016/J.JNUCMAT.2021.153267.

[30] C. Baker. “The fission gas bubble distribution in uranium dioxide from high temperature irradiated sghwr fuel pins”. In: *Journal of Nuclear Materials* 66 (3 May 1977), pp. 283–291. ISSN: 0022-3115. DOI: 10.1016/0022-3115(77)90117-9.

[31] R. J. White and M. O. Tucker. “A new fission-gas release model”. In: *Journal of Nuclear Materials* 118 (1 Aug. 1983), pp. 1–38. ISSN: 0022-3115. DOI: 10.1016/0022-3115(83)90176-9.

[32] Wahyu Setyawan et al. “Atomistic model of xenon gas bubble re-solution rate due to thermal spike in uranium oxide”. In: *Journal of Applied Physics* 124 (7 Aug. 2018), p. 14. ISSN: 10897550. DOI: 10.1063/1.5042770/15216147/075107_1_ACCEPTED_MANUSCRIPT.PDF. URL: /aip/jap/article/124/7/075107/155782/Atomistic-model-of-xenon-gas-bubble-re-solution.

[33] J. A. Turnbull et al. “The diffusion coefficients of gaseous and volatile species during the irradiation of uranium dioxide”. In: *Journal of Nuclear Materials* 107 (2-3 June 1982), pp. 168–184. ISSN: 0022-3115. DOI: 10.1016/0022-3115(82)90419-6.

[34] J.A. Turnbull, R.J. White, and C. Wise. “The diffusion coefficient for fission gas atoms in uranium dioxide”. In: International Atomic Energy Agency, Vienna (Austria), Sept. 1988, pp. 174–181. URL: http://inis.iaea.org/Search/search.aspx?orig_q=RN:21003206.

[35] Pekka Lösönen. “Modelling intragranular fission gas release in irradiation of sintered LWR UO2 fuel”. In: *Journal of Nuclear Materials* 304 (1 July 2002), pp. 29–49. ISSN: 0022-3115. DOI: 10.1016/S0022-3115(02)00856-5.

[36] M. S. Veshchunov and V. I. Tarasov. "Modelling of irradiated UO2 fuel behaviour under transient conditions". In: *Journal of Nuclear Materials* 437 (1-3 June 2013), pp. 250–260. ISSN: 0022-3115. DOI: 10.1016/J.JNUCMAT.2013.02.011.

[37] Christopher Matthews, Anders David Ragnar Andersson, and Cetin Unal. *Radiation Re-solution Calculation in Uranium-Silicide Fuels*. Los Alamos National Laboratory (LANL) LA-UR-16-22099, Jan. 2017. DOI: 10.2172/1341831. URL: http://www.osti.gov/servlets/purl/1341831/.

[38] D. R. Olander and D. Wongsawaeng. "Re-solution of fission gas – A review: Part I. Intragranular bubbles". In: *Journal of Nuclear Materials* 354 (1-3 Aug. 2006), pp. 94–109. ISSN: 0022-3115. DOI: 10.1016/J.JNUCMAT.2006.03.010.

[39] G. Martin et al. "Irradiation-induced heterogeneous nucleation in uranium dioxide". In: *Physics Letters A* 374 (30 July 2010), pp. 3038–3041. ISSN: 0375-9601. DOI: 10.1016/J.PHYSLETA.2010.05.033.

[40] J. A. Turnbull. "The distribution of intragranular fission gas bubbles in UO2 during irradiation". In: *Journal of Nuclear Materials* 38 (2 Feb. 1971), pp. 203–212. ISSN: 0022-3115. DOI: 10.1016/0022-3115(71)90044-4.

[41] M. S. Veshchunov. "On the theory of fission gas bubble evolution in irradiated UO2 fuel". In: *Journal of Nuclear Materials* 277 (1 Jan. 2000), pp. 67–81. ISSN: 0022-3115. DOI: 10.1016/S0022-3115(99)00136-1.

[42] J. Spino et al. "Matrix swelling rate and cavity volume balance of UO2 fuels at high burn-up". In: *Journal of Nuclear Materials* 346 (2-3 Nov. 2005), pp. 131–144. ISSN: 0022-3115. DOI: 10.1016/J.JNUCMAT.2005.06.015.

[43] Michael WD Cooper et al. "Fission gas diffusion and release for Cr2O3-doped UO2: From the atomic to the engineering scale". In: *Journal of Nuclear Materials* 545 (Mar. 2021), p. 152590. ISSN: 0022-3115. DOI: 10.1016/J.JNUCMAT.2020.152590.

[44] W. Wiesenack. *HPR-383, Summary and Comparison of LOCA Tests with BWR Fuel in the Halden Reator Project Test Series IFA-650*. Halden Reactor Project, 2015.

[45] et al. Magnusson P. *STUDSVIK/N-19/105 STUDSVIK-SCIP III-253—Subtask 1.1: Fuel fragmentation, relocation and dispersal, Final Summary Report*. Studsvik Nuclear AB, 2020.

[46] Y. Pontillon et al. *Fission gas release under fast transient and LOCA conditions: Analytical devices implemented at Commissariat a l'Energie Atomique (IAEA-TECDOC–1320)*. International Atomic Energy Agency (IAEA), 2002. URL: https://inis.iaea.org/search/search.aspx?orig_q=RN:34010869.

[47] Y Pontillon et al. "Experimental and theoretical investigation of fission gas release from UO2 up to 70 GWd/t under simulated LOCA type conditions: The GASPARD program". In: vol. 44. Sept. 2004. URL: https://www.researchgate.net/publication/286956984.

[48] G. Khvostov. "Analytical criteria for fuel fragmentation and burst FGR during a LOCA". In: *Nuclear Engineering and Technology* 52 (10 Oct. 2020), pp. 2402–2409. ISSN: 1738-5733. DOI: 10.1016/J.NET.2020.03.009.

[49] Katsumi Une, Shinji Kashibe, and Akira Takagi. “Fission Gas Release Behavior from High Burnup UO2 Fuels under Rapid Heating Conditions”. In: *https://doi.org/10.1080/18811248.2006.9711208* 43 (9 2006), pp. 1161–1171. ISSN: 00223131. DOI: 10.1080/18811248.2006.9711208. URL: https://www.tandfonline.com/doi/abs/10.1080/18811248.2006.9711208.

[50] J. Noirot et al. “Fission gas release behaviour of a 103 GWd/tHM fuel disc during a 1200 °C annealing test”. In: *Journal of Nuclear Materials* 446 (1-3 Mar. 2014), pp. 163–171. ISSN: 0022-3115. DOI: 10.1016/J.JNUCMAT.2013.12.002.

[51] J. P. Hiernaut and C. Ronchi. “Fission gas release and volume diffusion enthalpy in UO2 irradiated at low and high burnup”. In: *Journal of Nuclear Materials* 294 (1-2 Apr. 2001), pp. 39–44. ISSN: 0022-3115. DOI: 10.1016/S0022-3115(01)00469-X.

[52] M. Marcet et al. “High Burn up Structure Contribution to the Fission Gas Release under Transient Conditions”. In: Sept. 2009.

[53] L. Holt et al. “Sensitivity study on Xe depletion in the high burn-up structure of UO2”. In: *Journal of Nuclear Materials* 452 (1-3 Sept. 2014), pp. 166–172. ISSN: 0022-3115. DOI: 10.1016/J.JNUCMAT.2014.05.009.

[54] AN Kolmogorov. “On the Statistical Theory of Metal Crystallization”. In: *Izv. Akad. Nauk SSSR, Ser. Math* 1 (1937), pp. 335–360.

[55] Tyler J. Gerczak et al. “Restructuring in high burnup UO2 studied using modern electron microscopy”. In: *Journal of Nuclear Materials* 509 (Oct. 2018), pp. 245–259. ISSN: 0022-3115. DOI: 10.1016/J.JNUCMAT.2018.05.077.

[56] J. Noirot et al. “Post-irradiation examinations and high-temperature tests on undoped large-grain UO2 discs”. In: *Journal of Nuclear Materials* 462 (July 2015), pp. 77–84. ISSN: 0022-3115. DOI: 10.1016/J.JNUCMAT.2015.03.008.

[57] L. Noirot. “MARGARET: A comprehensive code for the description of fission gas behavior”. In: *Nuclear Engineering and Design* 241 (6 June 2011), pp. 2099–2118. ISSN: 0029-5493. DOI: 10.1016/J.NUCENGDES.2011.03.044.

[58] S. Brémier and C. T. Walker. “Radiation-enhanced diffusion and fission gas release from recrystallised grains in high burn-up {UO}{¡}2{}*nuclear fuel*”. In: *Radiation Effects and Defects in Solids* 157 (3 2002), pp. 311–322. ISSN: 10420150. DOI: 10.1080/10420150213000. URL: https://www.tandfonline.com/doi/abs/10.1080/10420150213000.

[59] K. Nogita and K. Une. “Irradiation-induced recrystallization in high burnup UO_2 fuel”. In: *Journal of Nuclear Materials* 226.3 (1995), pp. 302–310. DOI: 10.1016/0022-3115(95)00123-9.

[60] K. Kulacsy. “Mechanistic model for the fragmentation of the high-burnup structure during LOCA”. In: *Journal of Nuclear Materials* 466 (2015), pp. 409–416.

[61] Tommaso Barani et al. “Modeling high burnup structure in oxide fuels for application to fuel performance codes. Part II: Porosity evolution”. In: *Journal of Nuclear Materials* 563 (May 2022), p. 153627. ISSN: 0022-3115. DOI: 10.1016/J.JNUCMAT.2022.153627.

[62] Christopher Matthews et al. “Cluster dynamics simulation of xenon diffusion during irradiation in UO2”. In: *Journal of Nuclear Materials* 540 (Nov. 2020), p. 152326. ISSN: 0022-3115. DOI: 10.1016/J.JNUCMAT.2020.152326.

[63] MWD Cooper, C Matthews, and DA Andersson. *Gas evolution in high-burnup fuel and its impact on fuel fragmentation*. Tech. rep. Los Alamos National Laboratory LA-UR-21-29789, Sept. 2021.

[64] MWD Cooper, C Matthews, and DA Andersson. *Extension of UO2 mechanistic fission gas evolution model in BISON to high-burnup structure based on knowledge of irradiation induced point defects from lower length scales*. Tech. rep. Los Alamos National Laboratory LA-UR-22-24250, Sept. 2022.

[65] L. O. Jernkvist and A. Massih. *Model for axial relocation of fragmented and pulverized fuel pellets in distending fuel rods and its effects on fuel rod heat load*. Tech. rep. SSM-2015:37. Stråll säkerhets myndigheten, 2015.

[66] J. Spino et al. “Stereological evolution of the rim structure in PWR-fuels at prolonged irradiation: Dependencies with burn-up and temperature”. In: *Journal of Nuclear Materials* 354 (1-3 Aug. 2006), pp. 66–84. ISSN: 0022-3115. DOI: 10.1016/J.JNUCMAT.2006.02.095.

[67] J. P. Hiernaut et al. “Fission product release and microstructure changes during laboratory annealing of a very high burn-up fuel specimen”. In: *Journal of Nuclear Materials* 377 (2 July 2008), pp. 313–324. ISSN: 0022-3115. DOI: 10.1016/J.JNUCMAT.2008.03.006.

[68] Katsumi Une, Shinji Kashibe, and Kimio Hayashi. “Fission Gas Release Behavior in High Burnup UO2 Fuels with Developed Rim Structure”. In: *https://doi.org/10.1080/00223131.2002.10875557* 39 (2002), pp. 668–674. ISSN: 00223131. DOI: 10.1080/00223131.2002.10875557. URL: https://www.tandfonline.com/doi/abs/10.1080/00223131.2002.10875557.

[69] M. Marcet et al. “In situ Characterization of UO2 Microstructure Changes During an Annealing Test in an Environmental Scanning Electron Microscope”. In: *MRS Online Proceedings Library (OPL)* 1215 (2009), pp. 157–162. ISSN: 0272-9172. DOI: 10.1557/PROC-1215-V16-44. URL: https://www.cambridge.org/core/journals/mrs-online-proceedings-library-archive/article/abs/in-situ-characterization-of-uo2-microstructure-changes-during-an-annealing-test-in-an-environmental-scanning-electron-microscope/A13516F89AE0A076C6D9E2721040ABAD.

[70] M. Flanagan and P. Askeljung. “Observations of Fuel Fragmentation, Mobility and Release in Integral High-Burnup, Fueled LOCA Tests”. In: *Enlarged Halden Program Group Meeting 2011*. 2011.

[71] M. Helin and J. Flygare. *NRC LOCA tests at Studsvik, Design and construction of test train device and tests with unirradiated cladding material*. Tech. rep. STUDSVIK/N-11/130. Studsvik, 2012.

[72] Kyle A. Gamble et al. *Evaluation of Mechanistic and Empirical Models against Existing FFRD and LOCA Experimental Databases*. Tech. rep. Idaho National Laboratory, INL/RPT-22-69625, Sept. 2022.

[73] WJ Luscher, KJ Geelhood, and IE Porter. *Material Property Correlations: Comparisons between FRAPCON-4.0, FRAPTRAN-2.0, and MATPRO*. Tech. rep. PNNL-19417 Rev. 2. Pacific Northwest National Laboratory, Sept. 2015.

[74] W. F. Lyon. *Summary Report: Gd Thermal Conductivity Model Updates*. Tech. rep. ANA-P1400138-TN03 Rev. 2. Anatech Corp., 2015.

[75] H Kämpf and G Karsten. "Effects of Different Types of Void Volumes on the Radial Temperature Distribution of Fuel Pins". In: *Nuclear Technology* 9.3 (1970), pp. 288–300. DOI: 10.13182/NT70-A28783.

[76] D. D. Lanning and C. R. Hann. *Review of methods applicable to the calculation of gap conductance in zircaloy-clad UO2 fuel rods*. Tech. rep. BWNL-1894, UC-78B. Pacific Northwest National Laboratory, 1975.

[77] C. M. Allison et al. *SCDAP/RELAP5/MOD3.1 Code Manual, Volume IV: MATPRO-A Library of Materials Properties for Light-Water-Reactor Accident Analysis*. Tech. rep. NUREG/CR-6150, EGG-2720. Idaho National Engineering Laboratory, 1993.

[78] Michael R. Tonks, Pierre-Clément A. Simon, and Jacob Hirschhorn. "Mechanistic grain growth model for fresh and irradiated UO2 nuclear fuel". In: *Journal of Nuclear Materials* 543 (Jan. 2021), p. 152576. ISSN: 0022-3115. DOI: 10.1016/J.JNUCMAT.2020.152576.